

## SIM PLANETQUEST KEY PROJECT PRECURSOR OBSERVATIONS TO DETECT GAS GIANT PLANETS AROUND YOUNG STARS

ANGELLE TANNER<sup>1</sup>, CHARLES BEICHMAN<sup>1</sup>, RACHEL AKESON<sup>1</sup>, ANDREA GHEZ<sup>2</sup>, KONSTANTIN N. GRANKIN<sup>3</sup>, WILLIAM HERBST<sup>4</sup>, LYNNE HILLENBRAND<sup>5</sup>, MARCOS HUERTA<sup>6</sup>, QUINN KONOPACKY<sup>2</sup>, STANIMIR METCHEV<sup>2</sup>, SUBHANJOY MOHANTY<sup>7</sup>, L. PRATO<sup>8</sup>, MICHAL SIMON<sup>9</sup>

*Draft version November 9, 2021*

### ABSTRACT

We present a review of precursor observing programs for the SIM PlanetQuest Key project devoted to detecting Jupiter mass planets around young stars. In order to ensure that the stars in the sample are free of various sources of astrometric noise that might impede the detection of planets, we have initiated programs to collect photometry, high contrast images, interferometric data and radial velocities for stars in both the Northern and Southern hemispheres. We have completed a high contrast imaging survey of target stars in Taurus and the Pleiades and found no definitive common proper motion companions within one arcsecond (140 AU) of the SIM targets. Our radial velocity surveys have shown that many of the target stars in Sco-Cen are fast rotators and a few stars in Taurus and the Pleiades may have sub-stellar companions. Interferometric data of a few stars in Taurus show no signs of stellar or sub-stellar companions with separations of  $<5$  mas. The photometric survey suggests that approximately half of the stars initially selected for this program are variable to a degree ( $1\sigma > 0.1$  mag) that would degrade the astrometric accuracy achievable for that star. While the precursor programs are still a work in progress, we provide a comprehensive list of all targets ranked according to their viability as a result of the observations taken to date. By far, the observable that removes the most targets from the SIM-YSO program is photometric variability.

*Subject headings:* astrometry — stars: pre-main sequence — extrasolar planets

### 1. INTRODUCTION

The majority of the over 200 planets found to date have been detected using either radial velocity (RV) or transit studies in orbits ranging from less than 0.1 AU out to beyond 5 AU, with a wide range of eccentricities, and masses ranging from less than that of Uranus up to many times that of Jupiter (Butler et al. 2006). However, the host stars of these planets are mature main sequence stars which were chosen based on their having quiescent photospheres for the successful measurement of small Doppler velocities ( $<10$  m s<sup>-1</sup>). Similarly, stellar photospheres must be quiescent at the milli-magnitude level for transit detections since a Jupiter mass planet transiting a solar type star reduces the photometric signal by about 1.4%. Since young stars often have radial velocity fluctuations or rotationally broadened line widths of *at least* 500 m s<sup>-1</sup> and brightness fluctuations of many percent, RV measurements accurate to  $<100$  m s<sup>-1</sup> or transit observations cannot be used to detect planets

around young stars<sup>10</sup>. A few potentially planetary mass objects have been detected at 20-100 AU from young host stars ( $<10$  Myr) by direct, coronagraphic imaging, e.g 2MASSW J1207334-393254 (Chauvin et al. 2005) and GQ Lup (Neuhäuser et al. 2005). However, these companions are only inferred to be of planetary mass by comparison to uncertain evolutionary models that predict the brightness of “young Jupiters” as a function of mass and age (Wuchterl & Tscharnuter 2003; Baraffe et al. 2003; Burrows et al. 1997). Since dynamical determinations of mass are impossible for objects on such distant orbits, it is difficult to be sure that these are planets and not brown dwarfs. Nor is it even clear than the origin of these distant “young Jupiters” is due to same formation processes as planets found closer-in. Multiple fragmentation events (Boss 2001), rather than core accretion in a dense disk (Ida & Lin 2004), may be responsible for the formation of these distant objects. As a result of the selection biases of the radial velocity, transit and direct imaging techniques, we know little about the incidence of close-in planets around young stars, leaving us with many questions about the formation and evolution of gas giant planets.

Given the observational limitations and uncertainties that are inherent to radial velocity and direct imaging, micro-arcsecond astrometry is a feasible and direct method for estimating the masses of giant planets around stars in young clusters which lie at distances closer than 140 parsecs (Beichman et al. 2001). Equation (1) gives the astrometric amplitude,  $\phi$ , in units appropriate to the

<sup>10</sup> A number of groups are attempting RV observations in the near-IR since at these wavelengths it may be possible to improve on these limits and find a few “hot Jupiters” within 0.1 AU

<sup>1</sup> Michelson Science Center, Caltech, 770 S. Wilson Ave., Pasadena, CA 91125

<sup>2</sup> UCLA, Division of Astronomy, 430 Portola Plaza, Box 951547, Los Angeles, CA 90095-1547

<sup>3</sup> Astronomical Institute of the Uzbek Academy of Sciences, Tashkent, Uzbekistan, 700052

<sup>4</sup> Astronomy Department, Wesleyan University, Middletown, CT 06459.

<sup>5</sup> Caltech, MS 320-47, Pasadena, California 91125

<sup>6</sup> University of Florida, 211 Bryant Space Science Center, Gainesville, FL, 32611-2055

<sup>7</sup> Center for Astrophysics, Harvard University, 60 Garden Street Cambridge, MA 02138

<sup>8</sup> Lowell Observatory, 1400 W. Mars Hill Rd., Flagstaff, AZ 86001

<sup>9</sup> State University of New York at Stony Brook Dept. of Physics and Astronomy, Stony Brook, NY 11794-3800

search for planets around young stars:

$$\phi = 35 \frac{140pc}{D_{pc}} \frac{a_{AU}}{5.2AU} \frac{M_p}{M_J} \frac{M_\odot}{M_\star} \mu\text{as} \quad (1)$$

where  $\phi$  is the astrometric amplitude in  $\mu\text{as}$ ,  $D$  is the distance to the star in parsecs,  $a$  is the orbital semi-major axis of the planet in AU,  $M_p$  is the planet mass in Jupiter masses, and  $M_\star$  is the stars mass in solar masses. Thus, a Jupiter orbiting 5.2 AU away from a  $0.8 M_\odot$  star at the distance of youngest stellar associations (1-10 Myr) such as Taurus and Chamaeleon 140 pc away would produce an astrometric amplitude of  $44 \mu\text{as}$ . At the 25-50 pc distance of the nearest young stars (10-50 Myr) such as members of the  $\beta$  Pic and TW Hya moving groups, the same system would have an astrometric amplitude in excess of  $100 \mu\text{as}$ . Moving a Jupiter into a 1 AU orbit would reduce the signal by a factor of 5.2, or  $50 \mu\text{as}$  for a star at 25 pc and  $8 \mu\text{as}$  for one in Taurus. Table 1 lists the star formation regions and young moving groups being included in the SIM-YSO survey, a SIM PlanetQuest key project aimed at detecting Jupiter-mass planets around young stars. Since SIM will be able to detect astrometric signals with a Single Measurement Accuracy (SMA) of  $4 \mu\text{as}$  ( $1\sigma$ ) in a fairly quick ‘‘Narrow Angle (NA)’’ observation and  $11 \mu\text{as}$  in single ‘‘Wide Angle (WA)’’ observation, a search for gas giants falls well within SIMs capabilities for wide and narrow angle astrometry and forms the core of the SIM-YSO program. With SIM’s sensitivity it is reasonable to study stars brighter than  $R \sim 12$  mag to a level such that the expected astrometric amplitude of  $8 \mu\text{as}$  for stars at 140 pc is detected with  $2\sigma$  confidence in each measurement. This astrometric accuracy is appropriate for detecting planets of unknown orbital parameters with a series of approximately 75-100 1-D measurements (Sozzetti et al. 2003; Catanzarite et al. 2006).

Figure 1 shows orbital location (semi-major axis) and  $M \sin(i)$  for over 200 known planets orbiting nearby mature stars<sup>11</sup>. These planets were found using radial velocity measurements with noise levels as low as  $1 \text{ m s}^{-1}$ . However, for the the young stars considered here, the radial velocity measurements will be limited, even in the near-infrared, to  $100\text{-}500 \text{ m s}^{-1}$  (or greater) due to rapid rotation, veiling, and photospheric variability. Thus, we plot a RV sensitivity curve for planets orbiting a  $1 M_\odot$  star assuming a limiting accuracy of  $100 \text{ m s}^{-1}$ . For comparison, we plot the astrometric sensitivity curve for our SIM-YSO project where we demand that the minimum detectable planet have an amplitude twice the single measurement accuracy of  $4 \mu\text{as}$ . The curve is plotted for a  $1 M_\odot$  star located at the distance of Taurus (140 pc). For planets with periods greater than the nominal mission duration of 5 years, we have degraded the sensitivity as shown schematically in the plot. Finally, we estimate how a coronagraph on a 30-m telescope or an interferometer with an 85 m baseline, both operating at  $1.6 \mu\text{m}$  and reaching down to the Jovian mass range at orbital distances of 10 AU or greater would complement, but not replace, SIM observations.

In order to maximize the scientific yield of this SIM key project, a significant effort is required to gather in-

formation about the target stars prior to the launch of SIM. A careful vetting of the target list is required to reject stars that might be problematic due to the presence of starspots that might induce large astrometric offsets, to the presence of circumstellar emission from scattered light, or the presence of either visible and spectroscopic companions.

To ensure that we observe astrometrically stable systems, we have initiated a series of precursor observations to check for nearby infrared companions (§3), radial velocity variations due to unseen companions (§4), and photometric variability (§5). Table 2 summarizes those precursor programs presently being conducted along with the telescope and the principal investigator. In subsequent sections we summarize the different programs and give detailed results from a number of them. The SIM-YSO target list will continue to evolve as we add new stars for their scientific interest and remove stars due to one failing or another. In the end, we intend to have a complete sample in both stellar age and mass that will allow for a statistically significant study of planets around young stars.

This paper describes the present status of the SIM-YSO sample, the overall strategy for the precursor vetting program, and detailed results of one specific program, the Palomar AO survey aimed at identifying companions to the SIM-YSO targets in the Pleiades and Taurus. We will summarize briefly the progress being made on our photometric and radial velocity surveys of both the Northern and Southern targets and their implications for the SIM-YSO target sample.

## 2. THE SIM-YSO STELLAR SAMPLE OF YOUNG STARS

In a survey of  $\sim 200$  young stars we expect to find anywhere from 10-20 to 200 planetary systems depending on whether the 5-10% of stars with known radial velocity planets are representative of the younger planet population or whether all young stars have planets only to lose them to inward migration. The youngest stars in the sample (see Table 1) will be located in well known star-forming regions and will be observed in Narrow Angle mode which is capable of achieving single measurement accuracies of  $4 \mu\text{as}$ . Somewhat older stars, such as those in the  $\beta$  Pictoris and TW Hydrae Associations, are only 25-50 pc away, and can be observed less expensively in Wide Angle mode capable of a single measurement accuracy of  $< 11 \mu\text{as}$  (Unwin 2005).

We have set our sensitivity threshold to ensure the detection of Jupiter-mass planets in the critical orbital range of 1 to 5 AU. These observations, when combined with the results of the SIM planetary searches of mature stars, will allow us to test theories of planetary formation and early solar system evolution. By searching for planets around pre-main sequence stars carefully selected to span an age range from 1 to 100 Myr, we will learn at what epoch and with what frequency giant planets are found at the water-ice ‘‘snowline’’ where they are expected to form (Pollack et al 1996). This will provide insight into the physical mechanisms by which planets form and migrate from their place of birth, as well as their survival rate. With these observations in hand, we will provide data, for the first time, on such important questions as: What processes affect the formation and dynamical evolution of planets? When and where do

<sup>11</sup> Planet information from Schneider (2007)

planets form? What is initial mass distribution of planetary systems around young stars? How might planets be destroyed? What is the origin of the eccentricity of planetary orbits? What is the origin of the apparent dearth of companion objects between planets and brown dwarfs seen in mature stars? How might the formation and migration of gas giant planets affect the formation of terrestrial planets?

Our observational strategy is a compromise between the desire to extend the planetary mass function as low as possible and the essential need to build up sufficient statistics on planetary occurrence. About half of the sample will be used to address the “where” and “when” of planet formation. We will study classical T Tauri stars (cTTs) which have massive accretion disks as well as post-accretion, weak-lined T Tauri stars (wTTs). Preliminary estimates suggest the sample will consist of  $\sim 30\%$  cTTs and  $\sim 70\%$  wTTs, driven in part by the difficulty of making accurate astrometric measurements toward objects with strong variability or prominent disks. The extent to which this distribution of cTTs and wTTs survives the screening programs for photometric and dynamic stability will be addressed in §6. The second half of the sample will be drawn from the closest, young clusters with ages starting around 5 Myr to the 10 Myr thought to mark the end of prominent disks, and ending around the 100 Myr age at which theory suggests that the properties of young planetary systems should become indistinguishable from those of mature stars. The properties of the planetary systems found around stars in these later age bins will be used to address the effects of dynamical evolution and planet destruction (Lin et al. 2001).

We have adopted the following criteria in developing our initial list of candidates: a) stellar mass between 0.2 and 2.0  $M_{\odot}$ ; b)  $R < 12$  mag for reasonable integration times; c) distance less than 140 pc to ensure an astrometric signal greater than 6  $\mu\text{as}$ ; d) no companions within  $2''$  or 100 AU for instrumental and scientific considerations, respectively; e) no nebulosity to confuse the astrometric measurements; f) variability  $\Delta R < 0.1$  mag; and g) a spread of ages between 1 Myr and 100 Myr to encompass the expected time period of planet-disk and early planet-planet interactions. With proper selection, the effect of various astrophysical disturbances can be kept to less than the few  $\mu\text{as}$  needed to detect Jupiter-mass planets at  $\sim 50$ -140 pc.

The initial SIM-YSO sample (see Table 13) consists of stars in the well known star-forming regions and close associations. Figure 2 shows histograms of the properties of the stars in the sample including distance, V magnitude and age. The stars included in the initial sample have been screened for binarity in either imaging (Stauffer et al. 1998; Lowrance et al. 2005) or spectroscopic surveys (White & Ghez 2001; Mathieu et al. 1997; Steffen et al. 2001).

### 3. HIGH CONTRAST DIRECT IMAGING

We begin by presenting the results of a companion survey to those SIM-YSO targets in our Taurus and Pleiades

TABLE 1  
SIM-YSO SAMPLE

Cluster	Age [Myr]	Distance [pc]	# stars
Beta Pic	20	10-50	16
Chameleon	1-10	140	8
Eta Cha	4-7	100	2
Horologium	30	60	12
IC2391	53	155	12
Ophiuchus	2	160	5
Pleiades	125	130	14
TW Hydra	10	60	15
Taurus-Aureiga	2	140	25
Tucanae	20	45	20
Upper Sco	1-10	145	49
Sco Cen	1-25	130	81

TABLE 2  
PRECURSOR PROGRAMS

Program	Telescope	PI
AO Imaging (North)	Palomar	Tanner
AO Imaging (South)	VLT	Dumas
Speckle Imaging (North)	Keck	Ghez/Konopacky
V <sup>2</sup> (North)	Keck	Akeson
RV Survey (North)	McDonald	Prato
RV Survey (South)	CTIO/Magellan	Mohanty
Photometry (North)	Maidanak	Grankin
Photometry (South)	SMARTS	Simon

samples (see Table 3). Companions within the  $1''.5$  field-of-view of the SIM interferometer which have magnitudes within  $\Delta V \sim 4$  (M. Shao, private comm.) could cause a bias in the position of the fringe used to make the astrometric measurements. Additionally, a massive, unknown stellar companion will induce astrometric perturbations complicating the astrometric solution for a planet around the primary star. To look for common proper motion companions to the SIM-YSO stars, we have conducted an adaptive optics (AO) coronagraphic imaging survey around 31 stars in the Taurus (2 Myr, 140 pc, Kenyon et al. 1994) and Pleiades (120 Myr, 135 pc, Stauffer et al. 1998; Pan et al. 2004) clusters with the PALAO adaptive optics system and its near-infrared camera, PHARO, on the Hale 200-inch telescope at Palomar (Hayward et al. 2001). These data will reveal the presence of stellar and brown dwarf companions located between  $\sim 50$  and 1000 AU, and, in the case of the youngest stars in these systems ( $\sim 2$  Myr), will be sensitive to hot, young planets with masses in the range of 10-20  $M_J$  (Burrows et al. 1997; Baraffe et al. 2003).

In the process of searching for unseen companions around these stars, we are also addressing planet formation issues. By investigating whether the “brown dwarf desert” observed for separations of  $< 5$  AU around main sequence stars (Marcy et al. 2000) also exists at larger separations for young stars, we can test whether brown dwarfs are formed at this separation and subsequently migrate inward and are destroyed by falling onto the star. In this case we might find that T-Tauri stars have a larger population of brown dwarfs than main sequence stars at these separations.

TABLE 3  
PALOMAR TARGET SAMPLE

Target	V [mag]	2MASS $K_s$ [mag]	SpTy	Age [Myr]	Distance [pc]
HII 1032	11.1	9.16±0.02	G8	125	130
HII 1095	11.92	9.67±0.02	K0	125	130
HII 1124	12.12	9.86±0.02	K1	125	130
HII 1136	12.02	12.14±0.02	G8	125	130
HII 1275	11.47	9.53±0.02	G8	125	130
HII 1309	9.58	8.28±0.02	F6	125	130
HII 1514	10.48	8.95±0.02	G5	125	130
HII 1613	9.87	8.57±0.02	F8	125	130
HII 1794	10.2	8.89±0.02	F8	125	130
HII 1797	10.09	15.04±0.11	F9	125	130
HII 1856	10.2	8.66±0.02	F8	125	130
HII 2366	11.53	9.55±0.02	G2	125	130
HII 430	11.4	9.47±0.02	G8	125	130
HII 489	10.38	8.87±0.02	F8	125	130
AA Tau	12.82	8.05±0.02	K7	2	140
BP Tau	11.96	7.74±0.02	K7	2	140
DL Tau	13.55	7.96±0.02	G	2	140
DM Tau	13.78	9.52±0.02	K5	2	140
DN Tau	12.53	8.02±0.02	M0	2	140
DQ Tau	13.66	7.98±0.02	M0	2	140
DR Tau	13.6	6.87±0.02	K5	2	140
GK Tau	12.5	7.47±0.02	K7	2	140
IP Tau	13.04	8.35±0.02	M0	2	140
IQ Tau	14.5	7.78±0.02	M0.5	2	140
IW Tau	12.51	8.28±0.03	K7	2	140
LkCa 19	10.85	8.15±0.02	K0	2	140
V1072 Tau	10.3	8.30±0.02	K1	2	140
V830 Tau	12.21	8.42±0.02	K7	2	140
V836 Tau	13.13	8.60±0.02	K7	2	140

### 3.1. Data Reduction and Analysis

The Palomar observations were obtained over three observing runs - Oct. 23, 2003; Dec. 4-6 2003; and Nov. 12-14 2005 - with good ( $0''.2$ ) to moderate ( $0''.5$ ) seeing throughout the nights. The PHARO/PALAO camera has a pixel scale of 25 mas pixel<sup>-1</sup> and a field-of-view of 25 arcseconds. Each target was observed with the  $0''.97$  diameter occulting spot placed over the star with integration times of 60 seconds each and multiple (10-20) images collected per target. Sky images were also taken adjacent to each set of target images by offsetting  $30''$  from the target in the four cardinal directions. For flux calibration, observations of the target stars were taken with the star offset from the coronagraph in a five point dither pattern to allow for adequate sky subtraction. To improve observing efficiency, those stars with similar magnitudes and colors were paired together to act as each other's point spread function. Two sets of known binary stars with high quality orbital solutions (WDC 09008+4148 and WDC 23052-0742) were also observed to provide an accurate determination of the plate scale and image orientation. During these observations, each binary was placed in multiple positions over the field of view of the camera.

All the images were sky-subtracted, flat-fielded and corrected for bad-pixels. We utilized a number of methods for image registration prior to PSF subtraction. The best method involved using the centroid of either the waffle pattern or the "Poisson" spot (Metchev 2005). Using these methods we were able to achieve a registration accuracy of 2.3 and 0.7 pixels, respectively, which is compa-

ble to the accuracy achieved in a similar survey using the same instrument (Metchev et al. 2004). After registration, the median of each image stack was calculated to produce the final image (see Figure 3). The images of those target stars with similar magnitudes and colors are paired and subtracted to produce a difference image intended to reduce the residual flux within one arcsecond of the coronagraphic spot. Prior to subtraction, each pair of images was scaled to have the same peak flux within the coronagraph halo to ensure a minimal residual flux after subtraction. Figure 4 shows the difference image of GK Tau and V830 Tau with a bright companion candidate next to GK Tau.

A thorough visual inspection of both the median-averaged, coronagraphic images and the difference images was performed to identify all potential companions. All visual companions identified in these images are listed in Table 4 along with their distance from the center of the coronagraph, position angle and magnitude difference compared to the target star. The coronagraphic images have been flux calibrated using the images taken with the primary star off-set from the coronagraph while accounting for a difference in integration time and the well-defined neutral density filter used for the off-spot images (Metchev et al. 2004). The magnitudes for both the primary stars in the off-spot images and the companions in the coronagraphic images are estimated from aperture photometry with an aperture of  $0''.9$  and sky annulus of  $1''.1$ - $1''.4$ . The  $K_s$  band magnitudes of the primaries were taken from the Two Micron All-Sky Survey (Cutri et al. 2006). Since many of the target stars are variable in the optical, the near-infrared photometric calibration may be uncertain although these stars are typically 2-3 times less variable in the infrared than the visible (Eiroa et al. 2002).

### 3.2. Results

In Taurus and the Pleiades, 10 out of 16 of the targets (63%) and 5 out of 14 (36%), respectively, have visual companions within the  $25''$  ( $\sim 1750$  AU) field-of-view. Almost all of the companions lie  $>2$  arcseconds away from the target corresponding to a distance greater than 300 AU. To estimate the sensitivities of our images as a function of distance from the star, we employ "PSF planting" in which a PSF corresponding to an object of known brightness is inserted into the image to determine whether it is detectable. A PSF extracted from the off-spot image of each target is sky subtracted, normalized, multiplied by an array of contrast values ( $\Delta K_s = 7.7$ - $15.1$  mags) and placed at a range ( $0$ - $5''$ ) of distances from the target at random position angles. We completed 10,000 iterations of the PSF planting algorithm to fill out the parameter space of contrast and distance from the primary star. To determine whether the planted star is detected, the image is cross-correlated with a flux normalized PSF. The correlation values are binned according to the distance of the PSF from the star in increments of  $0''.1$ . For each distance bin we estimate the minimum PSF intensities which resulted in a correlation value of 0.9 or higher. The intensities are converted into magnitudes using the flux calibration from the off-spot image and the 2MASS  $K_s$  magnitude of the star. Figure 5 plots the largest  $K_s$  magnitude difference between the target star and planted PSF with a correlation of 0.9 as a function of distance

TABLE 4  
VISUAL COMPANIONS TO PLEIADES AND  
TAURUS TARGETS

Target	Separation ["]	PA [degrees]	$K_s$ [mag]
HII 1032	12.7	45.0	16.0
HII 1309	11.2	-27.2	15.0
HII 1309	12.1	108.8	15.2
HII 1797	6.6	-8.8	15.7
HII 489	13.4	144.4	17.1
AA Tau	5.9	98.6	15.2
BP Tau	3.1	-83.6	14.0
BP Tau	5.6	8.0	15.0
DL Tau	12.8	22.7	13.4
DL Tau	8.5	61.8	14.5
DL Tau	16.7	134.8	14.8
DL Tau	11.9	15.0	15.4
DQ Tau	7.3	149.6	15.3
GI Tau	8.3	1.7	14.6
GK Tau	2.4	62.1	12.1
IP Tau	3.7	124.3	15.1
IQ Tau	9.8	165.5	14.9
IQ Tau	13.9	-64.6	15.3
IQ Tau	10.7	-35.9	13.4
IQ Tau	10.2	-33.9	13.6
LkCa 19	4.3	-77.4	16.2
LkCa 19	11.8	-36.2	13.9
V830 Tau	7.1	-52.3	17.0
V830 Tau	11.2	58.3	15.8
V830 Tau	11.8	100.3	17.5
V830 Tau	7.8	146.1	17.7

from the star for all targets with calibration data. Table 6 lists the values of the faintest detectable  $K_s$  magnitudes at 0.5, 1, 2, 5 and 9 arcseconds. On average, we were able to detect sources with a magnitude contrast of  $\Delta K_S = 4-7$  mag at 2" and  $\Delta K_S \sim 8-10$  at 5". The range of image contrasts is due primarily to variations in seeing conditions throughout the night since all the targets had similar magnitudes and integration times.

Calibration binaries were used to estimate the plate scale of the PHARO camera. For the Oct 2004 data, we adopt a plate scale of  $25.11 \pm 0.04$  mas pixel<sup>-1</sup> estimated from 3 different binary stars (WDS 09006+4147, WDS 18055+0230, WDS 20467+1607) that were observed very close to our observations using the same instrument (Oct 4-5, 2004, Metchev 2005). For the 2005 data we estimate a plate scale of  $25.21 \pm 0.36$  mas pixel<sup>-1</sup>. This plate scale and its uncertainty comes from the average and standard deviation of the separation of one binary (WDS 09006+4147) placed in multiple positions across the field of view after correction for the known distortion in the camera.

To estimate the position of the occulted target star in these images, we use the waffle pattern inherent to every PSF (see Figure 3). Each waffle pattern consists of four points in a box pattern around the star. The center of the coronagraphic PSF is determined from the intersection of the two diagonal lines fitted to the centroid positions of the four peaks in the waffle pattern. Using this method, we are able to determine the position of the star to within 0.35 pixels estimated from the standard deviation of the stellar position in a stack of sub-frames. The positions of the companion candidates are estimated from their centroids and have errors of 0.5-1 pixels depending on the brightness of the companion, seeing conditions and telescope drift. The pixel positions for all primaries and

their companions are corrected for the distortion determined for the PHARO camera (Metchev 2005). The errors in the stellar position and PHARO pixel scale are propagated into the error of the offsets of the companion candidates from their primaries.

Figure 6 plots the offset in RA and Dec of companion candidates to BP Tau, IP Tau, GK Tau, and LkCa 19. These four sources all have objects within at least 4.5 arcseconds (675 AU). While the probability of these companion candidates being background sources goes up with their separation from the target star, the discovery of a number of brown dwarf companions at wide separations (>200 AU) makes these companion candidates worth investigating further. The crosses denote the positional offsets at the observing epochs of the Palomar data (2004, 2005) as well as data taken from Hubble Space Telescope (HST) WFPC2 and NICMOS data when available. The HST data was collected in 1999 as part of a program to detect faint debris disks (Krist et al. 2000) and therefore provides a long time baseline for the determination of common proper motion. In most cases, the target star in the WFPC2 data is saturated and the position of the star is estimated from the intersection of the diffraction spikes. The size of the crosses denote the  $3\sigma$  positional uncertainties ( $1\sigma \sim 12$  mas for the Palomar data and  $1\sigma \sim 3$  mas for the WFPC2 data, J. Krist, private comm.) The curvy solid lines depict the changes in the offsets expected if the companion were a stationary, background object. The dotted lines represent the errors in the published proper motions (Frink et al. 1997). If the companions are associated with the target stars, the offsets would coincide with one another at all epochs since the objects would share the same space motions. Table 5 lists the reduced chi-squared values estimated from the positional data and uncertainties. Two hypotheses are tested - common proper motion and non-common proper motion. In the first scenario the  $\chi^2$  is derived from the assumption that all the data points should lie on top of the first epoch (1999) data point. For the second scenario, the  $\chi^2$  is derived from the assumption that the data points should lie on the vector produced by the change in the offset between the science target and stationary background star. The uncertainties for this case include both the positional uncertainties and the uncertainty in the proper motion of the T Tauri star (Frink et al. 1997). An unmodeled source of uncertainty that may inflate the  $\chi^2$ s in the second scenario is the unknown proper motion of the companions. Based on this analysis, we conclude that there is evidence for common proper motion for the companion to GK Tau, evidence for non-common proper motion for the companion to BP Tau and ambiguous evidence for either scenario for IP Tau and LkCa19. These last two sources would benefit from more accurate positional data and a longer time baseline. If the GK Tau companion is truly a physical companion, then based on its  $K_s$  magnitude it would be roughly a M2-3 star with mass  $\sim 0.5 M_\odot$ .

We have begun a similar high contrast imaging survey of the SIM-YSO targets in the Upper Sco subgroup of the Sco Cen association (1-2 Myr, 145 pc) using the NACO camera on the VLT. The NACO camera has been used to discover a number of low-mass companions including 2M1207 and GQ Lupi (Neuhäuser et al. 2005; Chauvin

TABLE 5  
REDUCED  $\chi^2$  VALUES FROM COMMON AND NON-COMMON PROPER MOTION FITS

Target	Reduced $\chi^2_{CommonPM}$	Reduced $\chi^2_{Non-commonPM}$
BP Tau	26	2.5
GK Tau	1.4	4.1
IP Tau	4.2	4.4
LkCa19	43	6.3

TABLE 6  
PALOMAR IMAGING SENSITIVITIES

Target	$T_{int}$ [sec]	0".5	1"	2"	5"	9"
HII 1032	1200	12.84	13.55	15.91	18.01	18.17
HII 1136	1200	14.26	14.99	16.74	17.86	17.65
HII 1797	1200	12.17	12.04	14.53	17.19	17.28
HII 1794	1200	12.18	12.53	14.70	17.78	17.87
HII 489	1200	14.68	13.93	16.20	17.57	17.76
AA Tau	1200	13.31	11.44	15.20	17.16	17.36
BP Tau	1200	11.08	11.65	14.26	17.41	17.57
CI Tau	1200	12.02	12.10	13.68	17.67	17.67
DL Tau	1200	12.51	13.17	15.24	17.22	17.20
DN Tau	900	12.80	10.91	14.13	17.13	17.18
DQ Tau	1200	12.84	13.24	15.01	17.49	17.39
GK Tau	1200	11.58	11.22	12.90	16.94	17.15
GI Tau	1200	12.00	12.25	14.16	17.26	17.34
IP Tau	1200	13.86	13.00	15.78	17.04	17.11
IQ Tau	1200	12.27	13.18	14.93	16.82	16.93
LkCa 19	900	12.46	12.55	14.93	17.97	18.22
V830 Tau	1200	13.59	14.85	17.09	20.15	20.36

et al. 2005). It has a pixel scale of  $27 \text{ mas pixel}^{-1}$ , a FOV of  $28''$  with the potential of achieving sensitivities of  $\Delta K_s$  of 10 at  $1''$  (Chauvin et al. 2004). So far, we have collected data on 20 targets with a number of them having companion candidates within one arcsecond. We will collect second epoch observations for these sources at a later date.

### 3.3. Comparison to Other Surveys

There have been a few other ground AO and space-based surveys for low-mass companions to young stars (1-200 Myr) which have found a few brown dwarfs with separations between 75 to 1000 AU. These surveys had sample sizes ranging from 30-100 targets with two surveys finding 2-3 brown dwarfs when targeting stars in nearby associations (Metchev 2005; Lowrance et al. 2005) and one survey finding no brown dwarfs when targeting X-ray selected T-Tauri stars in the Chamaeleon and Sco-Cen OB associations (Brandner et al. 2000). Metchev (2005) has estimated a completeness corrected percentage of brown dwarfs at  $\sim 7 \pm 3\%$  ( $1\sigma$  confidence) around F5-K5 stars with an age and separation range of 3-500 Myr and 30-1600 AU. Therefore our finding no very low-mass objects in a survey of 30 stars is consistent with previous programs given the stated uncertainties. Whether there is a significant dearth of brown dwarfs or planetary mass objects around young stars still requires a larger sample of targets with similar sensitivities to allow for a direct comparison of detection statistics.

Stellar multiplicity surveys of star formation regions such as Taurus and the Pleiades have revealed binary

companion fractions of 60% (over 20-500 AU) and 30% (over 1-900 AU), respectively (Ghez et al. 1993; Bouvier et al. 1997). However, we used these and other surveys mentioned previously (see §2) to remove stars with stellar companions within two arcseconds in defining our initial sample. Thus it is not surprising that our survey did not add to the statistics for stellar multiplicity in these clusters.

### 3.4. Speckle Imaging and Additional AO imaging of the Taurus Sample

To complement the adaptive optics survey at Palomar, a number of the targets in the sample have been observed using high resolution imaging techniques at the Keck observatory. The purpose of this project was to look for companions at separations too close to be resolved with Palomar, and too wide to be detected via spectroscopic techniques. A summary of the results of this portion of the project is given in Table 8.

In total, seventeen objects in Taurus, TW Hydrae, or AB Doradus were surveyed at Keck. Three of these were imaged using speckle interferometry at K-band ( $2.2 \mu\text{m}$ ) on Keck I, and fourteen were observed using adaptive optics and K' ( $2.3 \mu\text{m}$ ) or L'-band ( $3.5 \mu\text{m}$ ) on Keck II. The dates of these observations are given in Table 8, along with the total exposure time on each target. For details on the data reduction and analysis of both the speckle and the AO data taken at Keck, please see Konopacky et al (2007).

For all 17 sources, no companions were found to within  $0''.05$ . For each source we estimated our sensitivity to companions by finding the limiting detectable flux ratio with respect to the source as a function of radius, and then using the models of Baraffe et al. (1998;  $\alpha = 1.0$ ) to convert these flux ratio limits into mass limits for the closest radius bin of  $0''.05$ . In general, the speckle measurements probe regions closer than  $0''.05$  with much greater sensitivity than AO, but given the combination of the two techniques for this survey, we cut off our official completeness at  $0''.05$ . We plan to observe the remaining targets visible from the Northern hemisphere with either Keck AO or speckle imaging and are beginning a survey of the targets in the Southern hemisphere using Lucky imaging, a similar observational technique at optical wavelengths (Law et al. 2006).

## 4. INTERFEROMETRIC OBSERVATIONS OF STARS IN TAURUS AND THE PLEIADES

The Keck Interferometer (KI) was used to make near-infrared, long-baseline interferometry observations of three sources in the Pleiades and five sources in Taurus. These observations are part of a long-term program to study the multiplicity fraction of these sources. In particular, the interferometer is sensitive to companions within 30 mas of the primary star and with a K magnitude difference of 3 magnitudes or less.

The observations were taken on 10 November, 2006 with KI configured in the 5-channel, K band (2.18 microns central wavelength) mode described in Colavita et al. (2003). Calibrators were chosen to match the targets in K magnitude and were reduced with the standard parameters (Colavita et al 2003), including the ratio correction for imbalanced flux on the two paths of the interferometer. The calibrator sizes were all set to

0.1  $\pm$  0.05 mas diameter, but in all cases, the calibrator diameter did not contribute significantly to the final uncertainty. The primary KI data product is the normalized visibility amplitude squared, for which a value of 1 indicates an unresolved source. The uncertainty given is the quadrature combination of the scatter in the target measurement and the uncertainty in the system visibility (which in this case is dominated by the scatter in the calibrator measurements). Table 9 lists the targets, the numbers of integrations, the calibrated visibility and total uncertainty and the calibrators used for each target. The uncertainty varies due to the number of integrations and the difficulty in observing those sources with fainter  $V$  magnitudes.

All targets observed in this sample, except V830 Tau, are unresolved; i.e. consistent with a point source at this resolution. At the distance to Taurus or the Pleiades the central star will be unresolved ( $<0.1$  mas). Using the best uncertainties of 0.06, we can place limits on the size of the emission of 1.3 mas (1.8 AU) in diameter ( $3\sigma$ ) for a uniform disk or on the presence of over-resolved (diffuse) emission within the 50 mas field-of-view of  $<10\%$  ( $3\sigma$ ). Additional observational epochs are needed to constrain the multiplicity. V830 Tau has visibilities estimated from earlier epochs of data (2003, 2004, Akeson et al. 2005) which differ from the expected value for an unresolved source by a few sigma (see Table 9). Future observations of this star with KI are planned to determine the nature of the resolved emission.

## 5. RADIAL VELOCITY VETTING

Some of the target stars will have stellar or sub-stellar companions that are not detectable by direct imaging (separations  $<50$  AU). We are conducting a number of radial velocity (RV) surveys of potential SIM-YSO stars to determine whether the targets have unseen companions that might complicate the astrometric detection of planetary-mass objects. For example, a 20  $M_J$  companion in a 1 year orbit around a 0.8  $M_\odot$  star has an RV amplitude of 660  $m s^{-1}$ . At 140 pc, this object would produce an astrometric signature of 160  $\mu$ as that would swamp the signal from any lower-mass planets. Located just a few milli-arcseconds from its parent star, the brown dwarf companion would be undetectable by direct, non-interferometric imaging. The goal of the RV program is to achieve accuracies on the order of  $<500 m s^{-1}$  over 3-4 years depending on the  $v \sin(i)$  and photospheric instabilities of each star with the goal of getting limits on stellar and sub-stellar companions on orbits interior of 5 AU.

There are two radial velocity surveys presently being conducted on the SIM-YSO targets in both the Northern and Southern hemispheres. The Southern survey was begun in July 2003 using the echelle spectrograph (R=25,000) on the CTIO 4-m telescope (S. Mohanty, PI). All 42 of the targets in this survey were in the Sco-Cen association. Only one epoch of these targets have been collected to date because of the unfortunate retirement of this instrument on this telescope. Many of the stars in Sco-Cen turned out to be fast rotators ( $>10 km s^{-1}$ , see Table 7 and Figure 9) which is not surprising since, at 10-20 Myrs of age, there is ample time for the stars to spin-up due to stellar contraction.

The Northern survey began in October 2004, and used

TABLE 7  
 $V \sin(i)$  VALUES FOR SCO-CEN TARGETS

Target	$V \sin(i)$ [ $km s^{-1}$ ]	Target	$V \sin(i)$ [ $km s^{-1}$ ]
TYC8648-446-1	10	TYC8238-1462-1	25
TYC8283-264-1	10	TYC8654-1115-1	25
TYC8282-516-1	13	TYC8655-149-1	25
TYC8645-1339-1	15	TYC9245-617-1	25
TYC9246-971-1	15	TYC7833-2559-1	25
TYC7796-1788-1	15	TYC8295-1530-1	25
TYC9244-814-1	15	TYC7353-2640-1	25
TYC7319-749-1	15	TYC8636-2515-1	30
TYC8317-551-1	15	TYC8646-166-1	30
TYC8242-1324-1	18	TYC7310-2431-1	30
TYC8249-52-1	18	TYC8294-2230-1	30
TYC8259-689-1	18	TYC7824-1291-1	33
TYC8297-1613-1	18	TYC8652-1791-1	35
TYC7848-1659-1	18	TYC7852-51-1	40
TYC8640-2515-1	20	TYC8633-508-1	45
TYC8644-340-1	20	TYC8248-539-1	50
TYC7811-2909-1	20	TYC7333-1260-1	50
TYC8667-283-1	23	TYC7851-1-1	55
TYC7822-158-1	23	TYC7783-1908-1	63
TYC9212-2011-1	25	TYC8270-2015-1	65

the coude echelle spectrograph (R=60,000) on the 2.7-m Harlan J. Smith telescope at McDonald Observatory (L. Prato, PI). Survey targets are located in the Pleiades cluster and in the Taurus star forming region. To date, 51 objects have been observed at multiple epochs with an RV precision of 140  $m s^{-1}$ . This survey makes use of simultaneous BVR photometry to search for correlations between rotation and RV periods, indicative of star spot modulation rather than the presence of a low-mass companion. Initial results which include a few targets with potential companions or signs of starspots will be presented in a forthcoming publication (Huerta et al. 2007; Huerta et al. 2005).

## 6. PHOTOMETRIC MONITORING

The photospheric activity that affects radial velocity and transit measurements affects astrometric measurements as well, but, as we will now show, at levels consistent with the secure detection of gas giant planets with SIM. From measurements of photometric variability (Herbst et al. 1994; Bouvier & Bertout, 1989; Bouvier et al. 1995) plus Doppler imaging (Strassmeier & Rice 1998), T Tauri stars are known to have active photospheres with large starspots covering significant portions of their surfaces (Schussler et al. 1996), as well as hot spots due to infalling, accreting material (Mekaden 1998). Day-to-day changes arise primarily because of rotation whereas month-to-month variations reflect changes in the spot sizes and their distribution across the surface. Long term monitoring is essential because different stars have different levels of magnetic activity, and these levels can change with time. These effects can produce large photometric variations which can significantly shift the photocenter of a star. In the simplest approximation, a completely black starspot, covering a small fraction,  $\beta \ll 1$ , of a stellar hemisphere, will shift the photocenter by an angle

$$\Delta\phi(\theta) \sim \beta \sin\theta \cos\theta \frac{R_\star}{D_\star} = 33.4 \beta \frac{R_\star}{R_\odot} \frac{140 pc}{D_{pc}} \sin\theta \cos\theta \quad [\mu\text{as}] \quad (2)$$

where  $R_*$  is the stellar radius,  $D_*$  is the distance to the star, and  $\theta$  is the longitude of starspot relative to the line of sight. We have assumed that the spot is on the star’s equator and that the star is observed edge-on relative to its rotation axis. The shift in the photocenter,  $\Delta\phi(\theta)$ , will increase as the spot rotates away from a face-on longitude ( $\propto \sin\theta$ ), following the rotation of the star as the spot shrinks in projected area ( $\propto \cos\theta$ ) and eventually goes behind the star. Relative to the fractional change in stellar brightness,  $\Delta I/I(\theta) = \beta \cos\theta$  and averaging over  $-\pi/2 < \theta < \pi/2$ , we get a root mean square (rms) dispersion in the location of the photocenter (the “astrometric jitter”) given by,

$$\langle \Delta\phi \rangle = \alpha \left\langle \frac{\Delta I}{I} \right\rangle \frac{R_*}{D_*} = 1.8 \frac{R_*}{R_\odot} \frac{140 \text{ pc}}{D_{\text{pc}}} \frac{\Delta R(\text{mag})}{0.05 \text{ mag}} [\mu\text{as}] \quad (3)$$

where  $\alpha$  is a geometric term of order 1.1. A more careful analysis takes into account the fact that the spots are not completely black, but rather emit with a temperature of  $\sim 1,000$  K cooler than the photosphere, are located over a range of typically high latitudes, and that an ensemble of stars will be observed at random angles to the line of sight. A Monte Carlo simulation shows a linear relationship like that of Eqn (3), but with a smaller coefficient:

$$\langle \Delta\phi(\text{Monte Carlo}) \rangle = 0.9 \frac{R_*}{R_\odot} \frac{140 \text{ pc}}{D_{\text{pc}}} \frac{\Delta R(\text{mag})}{0.05 \text{ mag}} [\mu\text{as}] \quad (4).$$

For a typical T Tauri star radius of  $3 R_\odot$  in Taurus, we see that the astrometric jitter is less than  $3 \mu\text{as}$  for R-band variability less than or equal to  $0.05 \text{ mag}$  ( $1\sigma$ ). Thus, the search for Jovian planets with astrometric amplitudes greater than  $6 \mu\text{as}$  is possible for stars less variable than about  $0.05 \text{ mag}$  in the visible even without a correction for jitter that may be possible using astrometric information at multiple wavelengths. Other astrophysical noise sources, such as offsets induced by the presence of nebulosity and stellar motions due to disk induced non-axisymmetric forces are negligible for appropriately selected stars. Finally, it is worth noting that searching for terrestrial planets will be difficult until stars reach an age such that their photometric variability falls well below  $0.01 \text{ mag}$  and the corresponding astrometric jitter below  $1 \mu\text{as}$ . Even then, color dependent astrometric corrections may be needed for the most sensitive measurements.

Since young stars have active photospheres it is important that we assess the degree of photospheric activity to determine the best targets for the program. The SIM-YSO team has two separate programs conducting photometric monitoring of the sample targets in the Northern and Southern hemispheres. The Southern targets are being observed in R band ( $0.9 \mu\text{m}$ ) at CTIO using the SMARTS (Small and Medium Aperture Research Telescope System) program (M. Simon, PI) which is comprised of small ( $0.9\text{-}1.5$  meter) telescopes in the Southern Hemisphere. To date, they have observed 132 stars in the Sco-Cen and Upper-Sco associations. Figure 7 plots the R magnitudes of AA Tau and DN Tau taken with the SMARTS survey. The standard deviations of the photometry for these two sources is  $0.17$  and  $1.5$ , respectively, making the latter source a problematic SIM-YSO

target.

The Northern component of the SIM-YSO sample which includes stars in Taurus and the Pleiades has been monitored photometrically with small telescopes at the Maidanak Observatory (W. Herbst, PI; Grankin et al. 2007). Approximately ten data points are obtained on each star during each season to sample the range of the variability. The data are taken primarily in the B, V, and R bands, with a small amount taken in the U band. Forty-two stars are on the program and about 450 individual measurements have been obtained each season.

Out of those targets observed to date in both the Northern and Southern samples, 33% of them have photometric variability that produces astrometric noise greater than  $3 \mu\text{as}$  (or roughly  $1\sigma \sim 0.05 \text{ mag}$ ) in either the V or R band (see Table 15). Simultaneous monitoring of the variable stars both photometrically and with radial velocity measurements during the SIM observations might allow us to model the jitter and derive accurate astrometry. Those targets exhibiting significant amounts of photometric variability will be monitored further to assess whether they should remain in the target list or regulated to Wide Angle observations which will be sensitive to Jupiter mass planets further than one AU from the star.

## 7. DISCUSSION

Through a series of precursor programs to observe all of the stars in the SIM-YSO target list it becomes clear that the observable affecting the viability of the targets the most is photometric variability. To date, 22% of the stars (33% of those stars observed) in the target list have variability which contributes more than  $3 \mu\text{as}$  of noise to the astrometric measurements. Table 13, which provides basic information on the entire SIM-YSO list, has been separated into “low variability”, “high variability” and “not observed” sections based on the degree of their variability and whether they have been observed to date. Each sublist is then ranked by the astrometric signal expected for a Jupiter mass planet at 1 AU from the stars which is listed under “Signal” in the table. To date, 67% of the sample has variability data with the remainder expected to be completed within the next year or two.

To replace those stars which might be lost to photometric variability, we will examine the literature for objects in other clusters or for newly classified T-Tauri stars. While many new young stars are being discovered in relatively nearby moving groups (i.e. Song et al. 2003), these typically have ages of  $10\text{-}25$  Myr. These stars can be observed inexpensively with SIMs Wide Angle mode and will probably not have problems of excessive variability. We will concentrate on finding bright enough replacement stars in the  $1\text{-}5$  Myr age range to avoid skewing our sample toward older stars.

### 7.1. Observing Scenarios and Reference Stars

While the nearer target stars ( $d < 50 \text{ pc}$ ) will have planetary astrometric signatures large enough to be detected by Wide Angle observations, more distant or more massive stars will have astrometric signatures on the order of  $6 \mu\text{as}$  requiring Narrow Angle observations. Narrow Angle observations require a set of at least three reference stars within the  $\sim 1^\circ 5$  field-of-view used for these observations. These reference stars must themselves be astro-

metrically stable to within  $< 4 \mu\text{as}$ . The best reference stars are K giants at distances  $> 500$  pc. There is an additional precursor program presently making photometric observations of the pool of reference stars available for every SIM-YSO target (or clusters of targets). When choosing the reference stars, we used a combined 2MASS-Tycho 2 catalog to select K giants based on visible-near IR colors as well as from reduced proper motions (RPM). The following selection criteria were also used to make the initial lists of reference stars: 1) separation from target  $< 1.25$  degrees, 2)  $0.5 < (J-K_s) < 1.0$ , 3)  $1.0 < (B_{Tycho} - V_{Tycho}) < 1.5$ , 4)  $V_{Tycho} < 10$ , and 5)  $\text{RPM} = K_s + 5 \log(\mu) < 1$ . While some of the reference stars have published spectral types, many stars do not have any spectral type at all. We have begun a program of verification of the luminosity classes of the photometrically selected sample using the SMARTS telescopes.

Observing the stars in Narrow Angle mode requires roughly five times more integration time than doing so in Wide Angle mode, primarily due to the necessity of observing 3-5 reference stars. Putting together the final program will require a balance between observing fainter, more distant and young objects in Narrow Angle mode versus the brighter, closer, and older stars in Wide Angle mode.

## 8. CONCLUSIONS

We have presented the results for a number of precursor programs aimed at creating a robust list of young stars to be observed as part of a Key project for the SIM PlanetQuest mission. This program will detect Jupiter-mass planets at distances of  $\sim 1\text{-}5$  AU from the star, thereby probing planet formation at distances comparable to where radial velocity planets are found around mature, main-sequence stars. The imaging surveys did

not find any stars with bright, nearby companions that could pose a problem for SIM; although we did find a potential M star companion  $2''.4$  away from GK Tau. The radial velocity surveys may have found one or two stars with close-in companions. In the near future, the RV surveys will be supplemented with high spectral resolution RV surveys in the near-infrared. These observations are not as affected by the photometric variability of the star and are expected to achieve RMS accuracies of down to  $100 \text{ m}^{-1}$  thereby allowing for the detection of lower mass objects. One selection effect we will have to guard against is losing too many of the youngest stars due to large photometric variations. We will continue to supplement our target list with additional stars which meet our basic criteria as well as investigate ways to mitigate astrometric jitter using multi-wavelength data from SIM itself.

LP and MH thank our colleagues C. Johns-Krull, P. Hartigan, and D. Jaffe for their collaboration on the McDonald Observatory project. Based on observations obtained at the Hale Telescope, Palomar Observatory, as part of a continuing collaboration between the California Institute of Technology, NASA/JPL, and Cornell University. The research described in this publication was carried out at the Jet Propulsion Laboratory, California Institute of Technology, under a contract with the National Aeronautics and Space Administration. This publication makes use of data products from the Two Micron All Sky Survey, which is a joint project of the University of Massachusetts and the Infrared Processing and Analysis Center/California Institute of Technology, funded by the National Aeronautics and Space Administration and the National Science Foundation.

## REFERENCES

- Akeson, R. L., et al. 2005, ApJ, 635, 1173  
 Baraffe, I., Chabrier, G., Barman, T. S., Allard, F., & Hauschildt, P. H. 2003, A&A, 402, 701  
 Beichman, C. A. 2001 in *Young Stars Near Earth: Progress and Prospects*, ASP Conference Series Vol. 244. Edited by Ray Jayawardhana and Thomas Greene. San Francisco: Astronomical Society of the Pacific, p.376  
 Boss, A. P. 2001, ApJ, 563, 367  
 Bouvier, J., Rigaut, F., & Nadeau, D. 1997, A&A, 323, 139  
 Bouvier, J., Covino, E., Kovo, O., Martin, E. L., Matthews, J. M., Terranegra, L., & Beck, S. C. 1995, A&A, 299, 89  
 Bouvier, J., & Bertout, C. 1989, A&A, 211, 99  
 Brandner, W., et al. 2000, AJ, 120, 950  
 Burrows, A., et al. 1997, ApJ, 491, 856  
 Butler, R. P., et al. 2006, ApJ, 646, 505  
 Catanzarite, J., Shao, M., Tanner, A., Unwin, S., & Yu, J. 2006, PASP, 118, 1322  
 Chauvin, G., et al. 2005, A&A, 438, L29  
 Chauvin, G., Lagrange, A.-M., Dumas, C., Zuckerman, B., Mouillet, D., Song, I., Beuzit, J.-L., & Lowrance, P. 2004, A&A, 425, L29  
 Colavita, M., et al. 2003, ApJ, 592, L83  
 Cutri, R., et al., 2006, AJ, 31, 1163  
 Eiroa, C., et al. 2002, A&A, 384, 1038  
 Frink, S., Röser, S., Neuhäuser, R., & Sterzik, M. F. 1997, A&A, 325, 613  
 Ghez, A. M., Neugebauer, G., & Matthews, K. 1993, AJ, 106, 2005  
 Grankin, K. N., Melnikov, S. Y., Bouvier, J., Herbst, W., & Shevchenko, V. S. 2007, A&A, 461, 183  
 Hayward, T. L., Brandl, B., Pirger, B., Blacken, C., Gull, G. E., Schoenwald, J., & Houck, J. R. 2001, PASP, 113, 105  
 Herbst, W., Herbst, D. K., Grossman, E. J., & Weinstein, D. 1994, AJ, 108, 1906  
 Huerta, M., et al. 2007, ApJ, in prep  
 Huerta, M., Prato, L., Hartigan, P., Johns-Krull, C. M., & Jaffe, D. 2005, Bulletin of the American Astronomical Society, 37, 1267  
 Kenyon, S. J., Dobrzycka, D., & Hartmann, L. 1994, AJ, 108, 1872  
 Konopacky, Q. M., Ghez, A. M., Rice, E. L., & Duchene, G. 2007, ArXiv Astrophysics e-prints, arXiv:astro-ph/0703567  
 Krist, J. E., Stapelfeldt, K. R., Ménard, F., Padgett, D. L., & Burrows, C. J. 2000, ApJ, 538, 793  
 Ida, S., & Lin, D. N. C. 2004, ApJ, 616, 567  
 Law, N. M., Hodgkin, S. T., & Mackay, C. D. 2006, MNRAS, 368, 1917  
 Lin, D. 2001, ASP Conf. Ser. 245: Astrophysical Ages and Times Scales, 245, 90  
 Lowrance, P. J., et al. 2005, AJ, 130, 1845  
 Marcy, G. W., & Butler, R. P. 2000, PASP, 112, 137  
 Mathieu, R. D., Stassun, K., Basri, G., Jensen, E. L. N., Johns-Krull, C. M., Valenti, J. A., & Hartmann, L. W. 1997, AJ, 113, 1841  
 Mekkaden, M. V. 1998, A&A, 340, 135  
 Metchev, S., 2005, PhD Thesis, California Institute of Technology  
 Metchev, S. A., & Hillenbrand, L. A. 2004, ApJ, 617, 1330  
 Neuhäuser, R., Guenther, E. W., Wuchterl, G., Mugrauer, M., Bedalov, A., & Hauschildt, P. H. 2005, A&A, 435, L13  
 Pan, S., Shao, M., Kulkarni, S., 2004, Nature, 427, 326  
 Preibisch, T., & Zinnecker, H. 1999, AJ, 117, 2381  
 Pollack, J. B., Hubickyj, O., Bodenheimer, P., Lissauer, J. J., Podolak, M., & Greenzweig, Y. 1996, Icarus, 124, 62  
 Schneider, J., 2007, <http://exoplanet.eu/>  
 Schuessler, M., Caligari, P., Ferriz-Mas, A., Solanki, S. K., & Stix, M. 1996, A&A, 314, 503

TABLE 8  
KECK IMAGING SENSITIVITIES

Object	Date Obs	Method (Sp or AO)	Total Exp. Int. Time [sec]	$\Delta K$ Lim 0''05	$\Delta K$ Lim 0''1	$\Delta K$ Lim $\geq 0''5$	Mass Lim 0''05 [ $M_{\odot}$ ]	Band
TWA 23	2005 May 27	Sp	78.1	2.9	3.7	6.9	0.10	K
TYC7660-0283	2005 May 27	Sp	78.1	3.9	4.1	6.5	0.08	K
GM Tau	1997 Oct 12	Sp	156.2	3.9	3.9	6.5	$\lesssim 0.02$	K
Anon 1	2005 Dec 12	AO	120	3.8	4.4	6.2	0.06	K
BP Tau	2005 Dec 12	AO	120	5.5	4.3	6.2	0.03	K
DG Tau	2005 Dec 12	AO	120	5.8	3.5	5.9	0.02	K
HD 283572	2005 Dec 12	AO	54.3	4.6	4.8	6.3	0.03	K
IP Tau	2005 Dec 12	AO	120	3.7	4.5	5.3	0.06	K
IQ Tau	2005 Dec 12	AO	120	5.0	4.7	5.9	0.03	K
V1072 Tau	2005 Dec 12	AO	120	5.1	5.5	6.5	0.03	K
DN Tau	2005 Dec 12	AO	120	4.7	5.1	6.2	0.03	K
V830 Tau	2005 Dec 12	AO	60	2.9	3.9	5.8	0.15	K
DR Tau	2005 Dec 12	AO	54.3	3.4	3.9	6.6	0.14	K
HIP 113579	2005 Jul 16	AO	3.0	3.7	3.5	5.7	0.24	L
HIP 113597	2005 Jul 16	AO	6.0	3.0	5.1	5.7	0.12	L
HIP 114066	2005 Jul 16	AO	6.0	2.9	3.0	5.3	0.09	L
HIP 115162	2005 Jul 16	AO	6.0	3.0	4.9	5.2	0.39	L

TABLE 9  
KECK INTERFEROMETRY RESULTS

Target	K mag	# ints	avg $V^2$	avg Sig	Calibrators
DN Tau	8.0	1	1.02	0.09	HD283444,HD283886
V830 Tau <sup>a</sup>	8.4	1	0.85	0.10	HD283668,HD282230,HD29334
V830 Tau <sup>b</sup>	8.4	1	0.89	0.07	HD283668,HD282230,HD29334
V830 Tau	8.4	1	1.08	0.13	HD283444,HD283886
V1171 Tau	9.2	2	0.98	0.05	HD24132,HD23289,HD284316
V1072 Tau	8.3	1	1.13	0.10	HIP19757,HD285816
V1075 Tau	8.9	1	1.08	0.10	HIP19757,HD285816
HD 282973	8.6	2	0.97	0.06	HD24132,HD23289,HD284316
HD 282971	8.7	2	0.99	0.06	HD24132,HD23289,HD284316
HD 23584	8.3	2	0.98	0.06	HD24132,HD23289,HD284316

<sup>a</sup> Observation from Oct. 16 2003

<sup>b</sup> Observation from Jan. 07 2004

Song, I., Zuckerman, B., & Bessell, M. S. 2003, ApJ, 599, 342  
 Sozzetti, A., Casertano, S., Brown, R. A., & Lattanzi, M. G. 2003,  
 PASP, 115, 1072  
 Stauffer, J. R., Schild, R., Barrado y Navascues, D., Backman,  
 D. E., Angelova, A. M., Kirkpatrick, J. D., Hambly, N., & Vanzi,  
 L. 1998, ApJ, 504, 805

Steffen, A. T., et al. 2001, AJ, 122, 997  
 Strassmeier, K. G., & Rice, J. B. 1998, A&A, 339, 497  
 Unwin, S. C. 2005, Astrometry in the Age of the Next Generation  
 of Large Telescopes, 338, 37  
 White, R. J., & Ghez, A. M. 2001, ApJ, 556, 265  
 Wuchterl, G., & Tscharnuter, W. M. 2003, A&A, 398, 1081

TABLE 10  
SIM-YSO SAMPLE

Name	Cluster	Distance [pc]	Spec Type	Age [Myr]	Star Mass <sup>a</sup> [M <sub>⊙</sub> ]	Signal [μas]	T-Tauri Class	V [mag]	2MASS K <sub>s</sub> [mag]
<b>Low variability targets</b>									
PreibZinn9964 <sup>b</sup>	USco	145	M1	0.1	0.3	23.68	...		8.36
51Eri	Beta Pic	29.8	F0V	20	1.5	21.51	...	5.22	4.54
PreibZinn9914	USco	145	M0.5	0.5	0.3	19.50	...		9.09
RECX10	Eta Cha	100	K6	7	0.6	17.48	WTT	12.53	8.73
PreibZinn9928	USco	145	M0	1	0.4	15.79	...		8.80
PreibZinn9913	USco	145	M0	1.2	0.4	15.07	...		8.88
PreibZinn9919	USco	145	K6	0.7	0.5	12.51	...		8.11
PreibZinn9974	USco	145	K4	0.5	0.6	10.36	...		8.46
PreibZinn9936	USco	145	K7	2.7	0.7	10.20	...		9.12
PreibZinn9967	USco	145	K5	1.1	0.7	10.05	...		8.56
PreibZinn9969	USco	145	K5	1.8	0.7	9.47	...		8.56
HII489	Pleiades	130	F8	125	...	9.25	...	10.38	8.87
HII1794	Pleiades	130	F8	125	...	9.25	...	10.20	8.89
HII2366	Pleiades	130	G2	125	...	9.25	...	11.53	9.55
TYC8283-2795-1	Sco-Cen(UCL)	130	...	...	...	9.25	WTT	10.79	8.98
PreibZinn9950	USco	145	K5	2.5	0.8	8.84	...		8.90
L1551-55	Tau Aur	140	K7	2	...	8.59	...	13.22	9.31
PreibZinn9939	USco	145	K4	2.2	0.8	8.29	...		8.73
HII1124	Pleiades	130	K3V	125	1.0	7.79	...	12.12	9.86
PreibZinn9958	USco	145	K2	1.2	0.9	7.62	...		8.43
HII1095	Pleiades	130	K0V	125	1.0	7.40	...	11.92	9.67
HII1309	Pleiades	130	F6V	125	1.0	7.40	...	9.58	8.28
HII1613	Pleiades	130	F8V	125	1.0	7.40	...	9.87	8.57
HII1797	Pleiades	130	F9V	125	1.0	7.40	...	10.09	15.04
HII1856	Pleiades	130	F8V	125	1.0	7.40	...	10.20	8.66
TYC8654-1115-1	Sco-Cen(LCC)	130		24	1.0	7.40	WTT	10.21	8.13
TYC8295-1530-1	Sco-Cen(UCL)	130	G5	21	1.0	7.40	WTT	10.98	8.90
PreibZinn9945	USco	145	K2	1.2	0.9	7.37	...	11.17	8.04
HD141569	none	35	B9.5e	5	4.0	6.87	...	7.11	6.82
TYC8667-283-1	Sco-Cen(LCC)	130	G3/G5V	23	1.1	6.72	WTT	9.31	7.62
TYC7783-1908-1	Sco-Cen(LCC)	130	G8IV:	18	1.1	6.72	WTT	9.82	7.51
TYC8258-1878-1	Sco-Cen(LCC)	130		15	1.1	6.72	WTT	10.62	8.27
TYC9244-814-1	Sco-Cen(LCC)	130	G3/G5III	22	1.1	6.72	WTT	10.21	8.40
TYC8270-2015-1	Sco-Cen(UCL)	130		17	1.1	6.72	WTT	10.91	8.69
TYC7851-1-1	Sco-Cen(UCL)	130	G9	17	1.1	6.72	WTT	10.63	8.36
TYC7353-2640-1	Sco-Cen(UCL)	130		18	1.1	6.72	WTT	10.72	8.67
CHXR8	Cham	140	G0	100	1.1	6.24	WTT	11.45	9.73
HII430	Pleiades	130	G8V	125	1.2	6.16	...	11.40	9.47
HII1032	Pleiades	130	A2	125	1.2	6.16	...	11.10	9.16
HII1136	Pleiades	130	G7V	125	1.2	6.16	...	12.02	12.14
HII1275	Pleiades	130	K0V	125	1.2	6.16	...	11.47	9.53
TYC8646-166-1	Sco-Cen(LCC)	130		11	1.2	6.16	WTT	10.50	8.18
TYC8636-2515-1	Sco-Cen(LCC)	130		11	1.2	6.16	WTT	10.58	8.12
TYC8633-508-1	Sco-Cen(LCC)	130	K2IV:+	16	1.2	6.16	WTT	9.41	7.65
TYC9245-617-1	Sco-Cen(LCC)	130		10	1.2	6.16	WTT	10.01	7.55
TYC8652-1791-1	Sco-Cen(LCC)	130	F6/F7	16	1.2	6.16	WTT	10.35	8.48
TYC8259-689-1	Sco-Cen(LCC)	130		14	1.2	6.16	WTT	10.48	8.10
TYC8248-539-1	Sco-Cen(LCC)	130	G1/G2	26	1.2	6.16	WTT	10.10	8.54
HD120411	Sco-Cen(UCL)	130	G1V	20	1.2	6.16	WTT?	9.79	8.16
V1009Cen	Sco-Cen(UCL)	130	G8/K0V	13	1.2	6.16	WTT?	10.18	7.95
TYC7310-2431-1	Sco-Cen(UCL)	130	G5	16	1.2	6.16	WTT	10.36	8.28
TYC8297-1613-1	Sco-Cen(UCL)	130		17	1.2	6.16	WTT	10.22	8.51
TYC7822-158-1	Sco-Cen(UCL)	130	K1	13	1.2	6.16	WTT	11.11	8.51
TYC7848-1659-1	Sco-Cen(UCL)	130	G5	15	1.2	6.16	WTT	10.36	8.21
HD140421	Sco-Cen(UCL)	130	G1V	17	1.2	6.16	WTT?	9.46	7.87
TYC8317-551-1	Sco-Cen(UCL)	130	G0	13	1.2	6.16	WTT	10.29	8.27
TYC7333-1260-1	Sco-Cen(UCL)	130	G1/G2V	18	1.2	6.16	WTT	9.58	8.07
PreibZinn9922	USco	145	G0	18	1.1	6.03	...		8.77
TYC9231-1566-1	Sco-Cen(LCC)	130	G3IV	12	1.3	5.69	WTT	9.23	7.18
TYC8263-2453-1	Sco-Cen(UCL)	130	F8/G0V	14	1.3	5.69	WTT	9.69	7.94
TYC7813-224-1	Sco-Cen(UCL)	130		14	1.3	5.69	WTT	10.55	8.39
TYC8683-242-1	Sco-Cen(UCL)	130		8	1.3	5.69	WTT	10.80	8.30
TYC7828-2913-1	Sco-Cen(UCL)	130		5	1.3	5.69	WTT	11.02	8.29
TYC7310-503-1	Sco-Cen(UCL)	130	K3	2	1.3	5.69	WTT	10.88	7.87
TYC7845-1174-1	Sco-Cen(UCL)	130	K1	3	1.3	5.69	WTT	10.61	7.93
TYC7349-2191-1	Sco-Cen(UCL)	130		1	1.3	5.69	WTT	11.09	8.29
PreibZinn9975	USco	145	G9	1	1.2	5.62	...	10.50	7.43
HII1514	Pleiades	130	G5V	125	1.4	5.28	...	10.48	8.95
HD140374	Sco-Cen(UCL)	130	G8V	8	1.4	5.28	WTT?	9.69	7.80
CHXR6	Cham	140	K2	1	1.3	5.28	CTT	11.22	7.31
PreibZinn9979	USco	145	G5	9	1.3	5.18	...		8.69
<b>High variability targets</b>									
PreibZinn9980	USco	145	M1	0.3	0.3	22.87	...		7.91
PreibZinn9940	USco	145	M2	0.4	0.3	22.10	...		8.61
PreibZinn9970	USco	145	M1	0.5	0.3	20.72	...		8.82
PreibZinn9955	USco	145	M1	0.5	0.3	20.09	...		8.10
PreibZinn9933	USco	145	M1	0.8	0.4	18.95	...		8.84

TABLE 11  
SIM-YSO SAMPLE CONT.

Name	Cluster	Distance [pc]	Spec Type	Age [Myr]	Star Mass <sup>a</sup> [M <sub>⊙</sub> ]	Signal [μas]	T-Tauri Class	V [mag]	2MASS K <sub>s</sub> [mag]
RECX4	Eta Cha	100	K7	4	0.5	18.49	WTT	12.79	8.62
PreibZinn9921	USco	145	M1	0.8	0.4	18.42			8.63
PreibZinn993	USco	145	M1	1	0.4	17.45			9.08
PreibZinn996	USco	145	M0	1	0.4	15.42			8.98
PreibZinn9963	USco	145	M0	1.8	0.5	14.74			8.44
DMTau	Tau Aur	140	K5V:e	2	0.5	14.61	CTT	13.78	9.52
PreibZinn9959	USco	145	M0	2	0.5	14.11			8.91
PreibZinn9962	USco	145	M0	2	0.5	14.11			8.92
CHXR29	Cham	140	A0pshe	...	0.5	13.74	CTT	8.44	5.94
CHXR18N	Cham	140	K1	...	0.5	13.74	WTT	12.05	7.77
CHXR68A	Cham	140	...	...	0.5	13.74	WTT	13.37	8.87
TCha	Cham	140	F5	...	0.5	13.74	CTT	11.86	6.95
PreibZinn9911	USco	145	K7	0.8	0.5	13.26			8.37
PreibZinn9916	USco	145	M0	2.9	0.5	13.26			9.27
DNTau	Tau Aur	140	K6V:e	0.46	0.6	12.26	CTT	12.53	8.02
IPTau	Tau Aur	140	M0:Ve	2	0.6	11.84	CTT	13.04	8.35
PreibZinn9926	USco	145	K7	1.8	0.6	11.05			8.92
DGTau	Tau Aur	140	GV:e	2	0.7	10.57	CTT		6.99
PreibZinn9961	USco	145	K5	1.8	0.7	9.47			8.62
UYAur	Tau Aur	140	G5V:e	2	0.7	9.28	CTT	12.40	7.24
BPTau	Tau Aur	140	K5V:e	0.6	0.8	9.16	CTT	11.96	7.74
GKTau	Tau Aur	140	2	2	0.8	9.16	CTT	12.50	7.47
AATau	Tau Aur	140	M0V:e	2	0.8	9.04	CTT	12.82	8.05
HQTau	Tau Aur	140	0.691831	2	0.8	9.04	CTT		7.14
IWTau	Tau Aur	140	K7V	2	0.8	9.04	WTT	12.51	8.28
DRTau	Tau Aur	140	K4V:e	2	0.8	9.04	CTT	13.60	6.87
V830Tau	Tau Aur	140	K7	2	0.8	8.92	WTT	12.21	8.42
DLTau	Tau Aur	140	GV:e	2	0.8	8.92	CTT	13.55	7.96
L1551-51	Tau Aur	140	K7	2	...	8.59		12.06	8.85
CITau	Tau Aur	140	GV:e	2	...	8.59		12.99	7.79
V836Tau	Tau Aur	140	K7V	2.1	0.8	8.59	WTT	13.13	8.60
PreibZinn9918	USco	145	K3	1	0.8	8.50			8.33
PreibZinn9942	USco	145	K5	2.9	0.8	8.50			8.37
PreibZinn9984	USco	145	K3	1	0.8	8.50			8.93
TYC8648-446-1	Sco-Cen(LCC)	130	19	0.9	8.22	WTT	11.18	8.79	
PreibZinn9968	USco	145	K2	1	0.8	7.89		11.65	7.69
SR4/V2058Oph	Ophiuchus	160	K5e	2	...	7.51		13.60	7.52
DoAr21Oph	Ophiuchus	160	B2V	2	...	7.51		13.82	6.23
Harol-16Oph	Ophiuchus	160	K3	2	...	7.51		12.59	7.61
V1121Oph	Ophiuchus	160	K5	2	...	7.51		11.25	6.96
V966Cen	Sco-Cen(LCC)	130	K1:V:+	...	1.0	7.40	WTT?	9.76	8.08
TYC7319-749-1	Sco-Cen(UCL)	130	K0	20	1.0	7.40	WTT	10.59	8.34
GITau	Tau Aur	140	K5e	2	0.9	7.39	CTT	13.50	7.89
PreibZinn991	USco	145	K3	3	0.9	7.37			9.43
PreibZinn9937	USco	145	K4	4	0.9	7.37			8.93
PreibZinn9976	USco	145	K1	1.2	1.0	6.98			8.49
V1072Tau/TAP35	Tau Aur	140	K1	2	1.0	6.87		10.30	8.30
TYC8640-2515-1	Sco-Cen(LCC)	130	20	1.1	6.72	WTT	10.77	8.73	
TYC8242-1324-1	Sco-Cen(LCC)	130	G0	16	1.1	6.72	WTT	10.38	8.14
TYC8238-1462-1	Sco-Cen(LCC)	130	K0	21	1.1	6.72	WTT	10.10	8.01
TYC8655-149-1	Sco-Cen(LCC)	130	19	1.1	6.72	WTT	10.31	8.37	
TYC8282-516-1	Sco-Cen(UCL)	130	19	1.1	6.72	WTT	10.68	8.54	
TYC7833-2559-1	Sco-Cen(UCL)	130	G6/G8III/IV	21	1.1	6.72	WTT	10.61	8.45
TYC8694-1685-1	Sco-Cen(UCL)	130	18	1.1	6.72	WTT	10.21	8.01	
PreibZinn9944	USco	145	K2	3.7	1.0	6.63			8.51
PreibZinn9973	USco	145	K0	0.8	1.0	6.57		11.00	7.49
PreibZinn9978	USco	145	K0	0.3	1.0	6.50		10.80	7.46
PreibZinn9929	USco	145	K3e	3	1.1	6.32		13.40	8.52
PreibZinn9954	USco	145	M3	3	1.1	6.32			8.86
TYC9246...71-1	Sco-Cen(LCC)	130	G	7	1.2	6.16	CTT	10.54	7.29
TYC9212-2011-1	Sco-Cen(LCC)	130	6	1.2	6.16	WTT	10.49	7.79	
TYC8644-340-1	Sco-Cen(LCC)	130	13	1.2	6.16	WTT	10.29	7.97	
TYC8645-1339-1	Sco-Cen(LCC)	130	5	1.2	6.16	WTT	10.82	7.73	
TYC8249-52-1	Sco-Cen(LCC)	130	K0/K1	13	1.2	6.16	WTT	10.48	8.13
HD117524	Sco-Cen(LCC)	130	G5/G6V	15	1.2	6.16	WTT?	9.84	7.83
TYC7796-1788-1	Sco-Cen(UCL)	130	K5	13	1.2	6.16	WTT	10.17	7.88
TYC7811-2909-1	Sco-Cen(UCL)	130	14	1.2	6.16	WTT	10.80	8.40	
TYC8283-264-1	Sco-Cen(UCL)	130	18	1.2	6.16	WTT	10.09	7.90	
TYC7824-1291-1	Sco-Cen(UCL)	130	G8IV:	15	1.2	6.16	WTT	9.80	7.81
TYC8294-2230-1	Sco-Cen(UCL)	130	G7	17	1.2	6.16	WTT	10.79	8.71
TYC7852-51-1	Sco-Cen(UCL)	130	F7V	18	1.2	6.16	WTT	9.05	7.69
PreibZinn9986	USco	145	K0	1.8	1.1	6.14			7.76
PreibZinn9983	USco	145	K0	2	1.1	6.03			8.51
PreibZinn9971	USco	145	K1	2.5	1.1	5.92		11.65	8.09
TYC8982-3213-1	Sco-Cen(LCC)	130	G1/G2V	13	1.3	5.69	WTT	9.49	7.60
HD105070	Sco-Cen(LCC)	130	G1V	13	1.3	5.69	WTT?	8.89	7.31
TYC8234-2856-1	Sco-Cen(LCC)	130	9	1.3	5.69	WTT	10.59	8.16	
TYC8633-28-1	Sco-Cen(LCC)	130	G2	15	1.3	5.69	WTT	9.49	7.77
HD108568	Sco-Cen(LCC)	130	G1	14	1.3	5.69	WTT?	8.89	7.29
HD113466	Sco-Cen(LCC)	130	G5V:	14	1.3	5.69	WTT?	9.18	7.36

TABLE 12  
SIM-YSO SAMPLE CONT.

Name	Cluster	Distance [pc]	Spec Type	Age [Myr]	Star Mass <sup>a</sup> [M <sub>⊙</sub> ]	Signal [μas]	T-Tauri Class	V [mag]	2MASS K <sub>s</sub> [mag]
TYC7833-2037-1	Sco-Cen(UCL)	130	K1	10	1.3	5.69	WTT	11.23	8.73
TYC7840-1280-1	Sco-Cen(UCL)	130	G9	9	1.3	5.69	WTT	10.57	8.29
PreibZinn9949	USco	145	G7	8.5	1.2	5.53			8.46
LkCa19	Tau Aur	140	K0V	2	1.3	5.49	WTT	10.85	8.15
PreibZinn9925	USco	145	G9	4	1.2	5.44		10.99	8.44
TYC8644-802-1	Sco-Cen(LCC)	130		6	1.4	5.28	WTT	10.21	7.66
HD108611	Sco-Cen(LCC)	130	G5V	10	1.4	5.28	WTT?	9.04	7.12
TYC7326...28-1	Sco-Cen(UCL)	130	K1	7	1.4	5.28	WTT	10.54	8.12
HD138995	Sco-Cen(UCL)	130	G5V	10	1.4	5.28	WTT?	9.39	7.52
TYC7842-250-1	Sco-Cen(UCL)	130		8	1.4	5.28	WTT	10.90	8.69
TYC7333-719-1	Sco-Cen(UCL)	130	G8	10	1.4	5.28	WTT	10.99	8.53
TYC7853-227-1	Sco-Cen(UCL)	130		8	1.4	5.28	WTT	11.05	8.65
<b>Yet to be measured targets</b>									
GJ803	Beta Pic	9.9	M1Ve	20	0.4	242.81		8.81	4.53
HD155555C	Beta Pic	31.4	M4.5	20	0.2	153.11		12.71	7.63
HIP23309	Beta Pic	26.3	K7V	20	0.5	81.25		10.02	6.24
HIP3556	Tuc	45	M1.5	20	0.3	71.23		11.91	7.62
GJ3305	Beta Pic	29.8	M0.5	20	0.5	64.53		10.59	6.41
CD-64d1208	Beta Pic	29.2	M0	20	0.6	54.88		9.54	6.10
GSC8056-0482	Hor	60	M3Ve	30	0.3	53.42		12.11	7.50
TWA8A	TW Hya	60	M2	10	0.3	53.42			7.43
TWA10	TW Hya	60	M2.5	10	0.3	53.42			8.19
TWA11B	TW Hya	60	M2.5	10	0.3	53.42		13.30	5.77
HIP107345	Tuc	45	M1	20	0.4	53.42		11.72	7.87
AOMen	Beta Pic	38.5	K3:V:	20	0.6	41.63		9.95	6.81
TWA7	TW Hya	60	M1	10	0.4	40.06		11.06	6.90
TWA13	TW Hya	60	M1Ve	10	0.4	40.06		11.50	7.49
HD35850	Beta Pic	26.8	F7V	20	1.0	35.88		6.30	4.93
HIP1993	Tuc	45	K7V	20	0.6	35.61		11.26	7.75
GSC8499-0304	Hor	60	M0Ve	30	0.5	32.05		12.09	8.72
TWA14	TW Hya	60	M0	10	0.5	32.05			8.50
TWA18	TW Hya	60	M0.5	10	0.5	32.05			8.85
HD3221	Tuc	45	K5V	20	0.8	26.71		9.56	6.53
GSC8497-0995	Hor	60	K6Ve	30	0.6	26.71		10.97	7.78
TWA6	TW Hya	60	K7	10	0.6	26.71		12.00	8.04
TWA1	TW Hya	60	K8Ve	10	0.6	26.71		10.92	7.30
TWA19B	TW Hya	60	K7	10	0.6	26.71			8.28
V343Nor	Beta Pic	39.8	K0V	20	1.0	24.16		8.14	5.85
HD202746	Tuc	45	K2Vp	20	0.9	23.74		8.97	6.40
TWA4	TW Hya	60	K5	10	0.7	22.89		8.89	5.59
TWA9A	TW Hya	60	K5	10	0.7	22.89		11.13	7.85
TWA17	TW Hya	60	K5	10	0.7	22.89			9.01
HD1466	Tuc	45	F8/G0V	20	1.0	21.37		7.46	6.15
HD186602	Tuc	45	F7/F8V	20	1.0	21.37		7.28	6.09
HD207575	Tuc	45	F6V	20	1.0	21.37		7.22	6.03
PPM366328	Tuc	45	K0	20	1.0	21.37		9.67	7.61
GSC8047-0232	Hor	60	K3V	30	0.8	20.03		10.87	8.41
CD-53d386	Hor	60	K3Ve	30	0.8	20.03		11.02	8.59
GSC8862-0019	Hor	60	K4Ve	30	0.8	20.03		11.67	8.91
BetaPic	Beta Pic	19.3	A5V	20	2.5	19.93		3.85	3.53
PZTel	Beta Pic	49.7	K0Vp	20	1.0	19.35		8.43	6.37
HD208233	Tuc	45	G8V	20	1.2	17.81		8.90	6.75
CCPhe	Hor	60	K1V	30	0.9	17.81		9.35	6.83
CD-65d149	Hor	60	K2Ve	30	0.9	17.81		10.19	8.01
HD172555	Beta Pic	29.2	A5IV-V	20	2.0	16.46		4.78	4.30
HD987	Tuc	45	G6V	20	1.3	16.44		8.76	6.96
HR9	Beta Pic	39.1	F2IV	20	1.5	16.39		6.19	5.24
CPD-64120	Hor	60	K1Ve	30	1.0	16.03		10.29	8.01
HD202917	Tuc	45	G5V	20	1.4	15.26		8.65	6.91
HD195627	Tuc	45	F1III	20	1.5	14.25		4.75	4.04
HD195961	Tuc	45	Fm	20	1.5	14.25		4.86	3.90
HD164249	Beta Pic	46.9	F5V	20	1.5	13.67		7.01	5.91
HD207129	Tuc	45	G0V	20	1.6	13.35		5.57	4.24
IQTau	Tau Aur	140	M2	2	0.5	13.21	CTT	14.50	7.78
HD181327	Beta Pic	50.6	F5/F6V	20	1.5	12.67		7.04	5.91
HD178085	Tuc	45	G0V	20	1.7	12.57		8.31	6.88
RXJ012320.9-572853	HOR	60	G6V	30	1.3	12.33		8.53	6.85
DQTau	Tau Aur	140	M0V:e	2	0.6	12.05	CTT	13.66	7.98
RXJ020718.6-531155	HOR	60	G5V	30	1.4	11.45		8.64	6.89
TWA19A	TW Hya	60	G3/G5Vp	10	1.4	11.45		9.07	7.51
RXJ020436.7-545320	HOR	60	F2V	30	1.5	10.68		6.45	5.45
HD200798	Tuc	45	A5/A6IV/V	20	2.0	10.68		6.69	6.07
GMTau	Tau Aur	140	M6.5	2	...	8.59			10.63
I045251+3016	Tau Aur	140	K5	2	...	8.59		11.60	8.13
Haro6-37	Tau Aur	140	K6	2	0.8	8.48	CTT	13.42	7.31
VXR03	IC2391	155	...	53	...	7.75		10.95	14.86
L36	IC2391	155	F6V	53	...	7.75		9.83	8.63
VXR31	IC2391	155	...	53	...	7.75		11.22	9.69
H21	IC2391	155	...	53	...	7.75		11.69	9.54
SHJM3	IC2391	155	K3e	53	0.8	7.75		12.63	9.69

TABLE 13  
SIM-YSO SAMPLE CONT.

Name	Cluster	Distance [pc]	Spec Type	Age [Myr]	Star Mass <sup>a</sup> [M <sub>⊙</sub> ]	Signal [μas]	T-Tauri Class	V [mag]	2MASS K <sub>s</sub> [mag]
ROX3/V2245Oph	Ophiuchus	160	M1	2	...	7.51		13.12	8.78
HR6070	Beta Pic	43	A0V	20	3.0	7.45		4.80	4.74
PreibZinn9985	USco	145	K2	2	0.9	7.13			8.18
HR136	Tuc	45	A0V	20	3.0	7.12		5.07	4.99
HR9062	Tuc	45	A1V	20	3.0	7.12		5.00	4.82
SHJM6	IC2391	155	K0	53	1.0	6.20		11.86	9.79
VXR62	IC2391	155		53	1.0	6.20		11.73	15.03
VXR67	IC2391	155		53	1.0	6.20		11.71	13.61
VXR16	IC2391	155		53	1.1	5.64		11.84	14.58
VXR72	IC2391	155	G9	53	1.1	5.64		11.46	9.59
HR126	Tuc	45	B9V	20	4.0	5.34		4.36	4.48
TWA11A	TW Hya	60	A0V	10	3.0	5.34		5.78	5.77

<sup>a</sup> The masses presented here are either taken from the literature or are estimated using the isochrones of D'Antona and Mazzitelli (1994)

<sup>b</sup> Preibisch & Zinnecker (1999)

TABLE 14  
STELLAR VARIABILITIES

Target	Peak to Peak	$\sigma_{stdev}$	Program	Target	Peak to Peak	$\sigma_{stdev}$	Program
HII1215	0.024	0.009	Maidanak	PreibZinn99 68	0.140	0.045	SMARTS
51 Eri	0.019	0.010	Maidanak	TYC7326-928-1	0.140	0.045	SMARTS
GJ3305	0.020	0.010	Maidanak	5251+3060	0.150	0.045	Maidanak
HII996	0.030	0.010	Maidanak	TYC8238-1462-1	0.150	0.045	SMARTS
HII489	0.029	0.012	Maidanak	CHXR 65	0.170	0.045	SMARTS
HII1309	0.037	0.013	Maidanak	DM Tau	0.136	0.046	Maidanak
CHXR 11	0.040	0.013	SMARTS	PreibZinn99 59	0.140	0.046	SMARTS
HD141569	0.056	0.013	Maidanak	TYC7319-749-1	0.180	0.046	SMARTS
HII1207	0.034	0.014	Maidanak	PreibZinn99 61	0.140	0.047	SMARTS
HII1797	0.044	0.014	Maidanak	PreibZinn99 1	0.140	0.047	SMARTS
HII1856	0.051	0.014	Maidanak	PreibZinn99 29	0.170	0.047	SMARTS
HII1095	0.050	0.015	Maidanak	PreibZinn99 37	0.140	0.048	SMARTS
HII1613	0.054	0.015	Maidanak	TYC8655-149-1	0.140	0.048	SMARTS
HD140374	0.060	0.015	SMARTS	TYC7853-227-1	0.140	0.048	SMARTS
HII2366	0.041	0.016	Maidanak	PreibZinn99 32	0.130	0.049	SMARTS
PreibZinn99 69	0.050	0.016	SMARTS	TYC8283-264-1	0.150	0.049	SMARTS
HII1794	0.055	0.016	Maidanak	HD149735	0.130	0.050	SMARTS
TYC9244-814-1	0.050	0.017	SMARTS	TYC7840-1280-1	0.170	0.051	SMARTS
TYC8259-689-1	0.060	0.017	SMARTS	TYC7842-250-1	0.130	0.052	SMARTS
HII430	0.048	0.018	Maidanak	TYC8644-340-1	0.130	0.052	SMARTS
TYC8270-2015-1	0.050	0.018	SMARTS	TYC8694-1685-1	0.150	0.052	SMARTS
HII1275	0.056	0.018	Maidanak	PreibZinn99 76	0.160	0.052	SMARTS
TYC7871-1282-1	0.070	0.018	SMARTS	TYC7833-2037-1	0.800	0.052	SMARTS
HII1514	0.059	0.019	Maidanak	TYC7852-51-1	0.140	0.053	SMARTS
HD149551	0.060	0.019	SMARTS	PreibZinn99 26	0.170	0.054	SMARTS
PreibZinn99 74	0.060	0.019	SMARTS	PreibZinn99 16	0.170	0.055	SMARTS
TYC8646-166-1	0.070	0.019	SMARTS	PreibZinn99 84	0.170	0.055	SMARTS
PreibZinn9 10	0.070	0.019	SMARTS	PreibZinn99 86	0.190	0.056	SMARTS
TYC7848-1659-1	0.060	0.020	SMARTS	TYC7824-1291-1	0.190	0.057	SMARTS
CHXR 37	0.070	0.020	SMARTS	PreibZinn99 23	0.150	0.058	SMARTS
CHXR 8	0.070	0.020	SMARTS	TYC8249-52-1	0.150	0.058	SMARTS
PreibZinn99 19	0.070	0.021	SMARTS	TYC8645-1339-1	0.170	0.058	SMARTS
TYC7353-2640-1	0.080	0.021	SMARTS	HD108611	0.180	0.058	SMARTS
RECX5	0.090	0.021	SMARTS	TYC7811-2909-1	0.150	0.062	SMARTS
TYC9245-617-1	0.060	0.022	SMARTS	TYC9212-2011-1	0.160	0.062	SMARTS
PreibZinn99 75	0.070	0.022	SMARTS	ROX3	0.180	0.062	SMARTS
TYC7828-2913-1	0.070	0.022	SMARTS	V1121 Oph	0.270	0.063	SMARTS
PreibZinn99 64	0.070	0.022	SMARTS	TYC7815-2029-1	0.220	0.064	SMARTS
TYC8633-508-1	0.080	0.022	SMARTS	TYC7858-830-1	0.170	0.065	SMARTS
TYC8636-2515-1	0.090	0.022	SMARTS	PreibZinn99 6	0.190	0.065	SMARTS
PreibZinn99 81	0.080	0.023	SMARTS	PreibZinn99 63	0.200	0.066	SMARTS
HII1032	0.068	0.024	Maidanak	TAP35	0.308	0.066	Maidanak
TYC7310-2431-1	0.080	0.024	SMARTS	TYC7796-1788-1	0.170	0.067	SMARTS
TYC8283-2795-1	0.080	0.024	SMARTS	PreibZinn99 40	0.180	0.067	SMARTS
TYC8667-283-1	0.090	0.024	SMARTS	RECX4	0.200	0.067	SMARTS
TYC7305-380-1	0.090	0.025	SMARTS	PreibZinn99 77	0.160	0.068	SMARTS
TYC7349-2191-1	0.090	0.025	SMARTS	PreibZinn99 3	0.200	0.068	SMARTS
TYC7310-503-1	0.080	0.026	SMARTS	CHXR 18N	0.210	0.068	SMARTS
PreibZinn99 66	0.080	0.027	SMARTS	SR4	0.200	0.069	SMARTS
PreibZinn99 82	0.080	0.027	SMARTS	TYC7333-719-1	0.240	0.069	SMARTS
TYC8297-1613-1	0.100	0.027	SMARTS	ROX43A	0.180	0.072	SMARTS
TYC9231-1566-1	0.100	0.027	SMARTS	Haro6-37	0.230	0.075	SMARTS
PreibZinn99 2	0.090	0.028	SMARTS	CHXR 66	0.220	0.076	SMARTS
TYC8258-1878-1	0.090	0.028	SMARTS	PreibZinn99 18	0.240	0.077	SMARTS
TYC8317-551-1	0.100	0.028	SMARTS	PreibZinn99 55	0.230	0.078	SMARTS
TYC8652-1791-1	0.100	0.029	SMARTS	V830 Tau	0.346	0.078	Maidanak
TYC7845-1174-1	0.110	0.029	SMARTS	PreibZinn99 70	0.230	0.079	SMARTS
CHXR 40	0.100	0.030	SMARTS	TYC8294-2230-1	0.230	0.079	SMARTS
PreibZinn99 13	0.100	0.030	SMARTS	L1551-51	0.258	0.079	Maidanak
PreibZinn99 45	0.100	0.030	SMARTS	V966 Cen	0.130	0.080	SMARTS
TYC7783-1908-1	0.110	0.030	SMARTS	PreibZinn99 11	0.230	0.081	SMARTS
PreibZinn99 17	0.110	0.030	SMARTS	HD105070	0.230	0.083	SMARTS
TYC8983-98-1	0.110	0.030	SMARTS	CHXR 29	0.260	0.083	SMARTS
PreibZinn99 58	0.090	0.031	SMARTS	TYC7813-224-1	0.080	0.084	SMARTS
TYC8295-1530-1	0.100	0.031	SMARTS	TYC8982-3213-1	0.250	0.085	SMARTS
TYC7822-158-1	0.110	0.031	SMARTS	IWTau	0.238	0.086	Maidanak
TYC7333-1260-1	0.110	0.031	SMARTS	V1056 Sco	0.230	0.087	SMARTS
V1009 Cen	0.090	0.032	SMARTS	TYC9246-971-1	0.240	0.088	SMARTS
PreibZinn99 39	0.090	0.034	SMARTS	PreibZinn99 25	0.250	0.088	SMARTS
HD140421	0.110	0.034	SMARTS	PreibZinn99 33	0.250	0.091	SMARTS
TYC8263-2453-1	0.110	0.034	SMARTS	PreibZinn99 54	0.240	0.092	SMARTS
PreibZinn99 14	0.120	0.034	SMARTS	PreibZinn99 49	0.210	0.093	SMARTS
LkCa19	0.163	0.034	Maidanak	TYC8242-1324-1	0.320	0.094	SMARTS
TYC8654-1115-1	0.120	0.035	SMARTS	PreibZinn99 80	0.260	0.097	SMARTS
TYC8640-2515-1	0.130	0.035	SMARTS	PreibZinn99 42	0.290	0.097	SMARTS
PreibZinn99-79	0.100	0.036	SMARTS	PreibZinn99 21	0.300	0.107	SMARTS
TYC8683-242-1	0.110	0.036	SMARTS	HQTau	0.233	0.109	Maidanak
PreibZinn99 28	0.110	0.037	SMARTS	CI Tau	0.298	0.114	Maidanak
PreibZinn99 60	0.110	0.037	SMARTS	IPTau	0.362	0.125	Maidanak
PreibZinn99 67	0.120	0.037	SMARTS	PreibZinn99 15	0.430	0.126	SMARTS
HII1124	0.100	0.038	Maidanak	TYC7817-622-1	0.380	0.127	SMARTS

TABLE 15  
STELLAR VARIABILITIES

Target	Peak to Peak	$\sigma_{stdev}$	Program	Target	Peak to Peak	$\sigma_{stdev}$	Program
PreibZinn99 27	0.140	0.038	SMARTS	BP Tau	0.457	0.129	Maidanak
PreibZinn99 62	0.140	0.038	SMARTS	UYAur	0.350	0.130	Maidanak
RECX6	0.150	0.038	SMARTS	SR10	0.370	0.131	SMARTS
DN Tau	0.165	0.038	Maidanak	DoAr 21	0.310	0.134	SMARTS
PreibZinn99 36	0.110	0.039	SMARTS	DG Tau	0.606	0.138	Maidanak
CHXR 6	0.120	0.039	SMARTS	PreibZinn99 78	0.350	0.139	SMARTS
HD120411	0.120	0.039	SMARTS	V836 Tau	0.417	0.142	Maidanak
RECX10	0.120	0.039	SMARTS	HD113466	0.390	0.149	SMARTS
TYC8248-539-1	0.120	0.039	SMARTS	GK Tau	0.692	0.183	Maidanak
PreibZinn9 22	0.110	0.040	SMARTS	PreibZinn99 73	0.550	0.188	SMARTS
TYC8319-1687-1	0.120	0.040	SMARTS	DL Tau	0.723	0.212	Maidanak
PreibZinn99 71	0.140	0.040	SMARTS	DH Tau	0.537	0.214	Maidanak
HD138995	0.150	0.040	SMARTS	GI Tau	0.597	0.216	Maidanak
L1551-55	0.126	0.041	Maidanak	TYC8633-28-1	0.180	0.226	SMARTS
TYC7833-2559-1	0.140	0.041	SMARTS	HD108568	0.550	0.233	SMARTS
PreibZinn99 83	0.130	0.042	SMARTS	PreibZinn99 44	0.670	0.262	SMARTS
TWA19	0.140	0.042	SMARTS	DR Tau	1.092	0.296	Maidanak
HD117524	0.140	0.043	SMARTS	AA Tau	1.499	0.454	Maidanak
TYC8644-802-1	0.140	0.043	SMARTS	TYC8234-2856-1	0.170	0.495	SMARTS
CHXR 68A	0.150	0.043	SMARTS	TYC8282-516-1	0.130	0.689	SMARTS
TYC7851-1-1	0.120	0.044	SMARTS	RECX2	2.150	0.808	SMARTS
TYC8648-446-1	0.150	0.044	SMARTS	TCha	2.430	0.850	SMARTS
PreibZinn99 50	0.120	0.045	SMARTS	HII1136	1.841	1.127	Maidanak

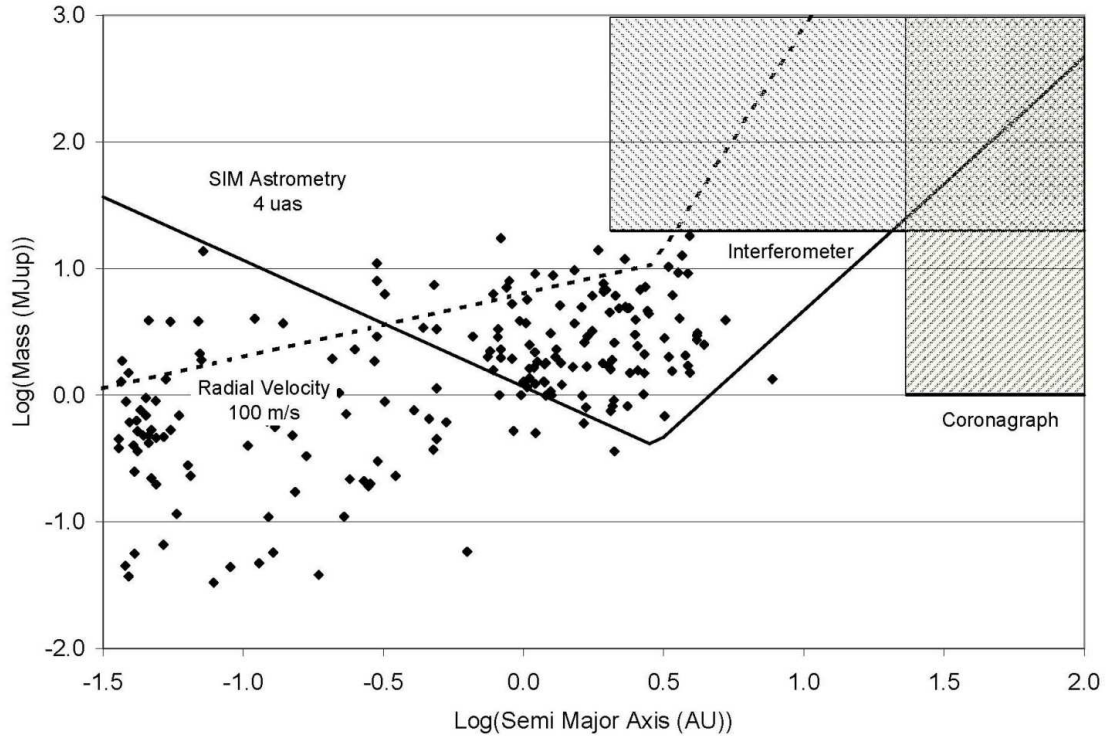


FIG. 1.— Plot of planet mass in  $M_J$  versus semi-major axis of the sensitivities expected from the SIM-YSO survey (solid-line) in addition to ground based coronagraph (labeled), interferometry (labeled) and radial velocity (dashed line) surveys of young stars. Also plotted are the properties of the known radial velocity planets (diamonds). All these sensitivity limits assume a distance of 140 pc.

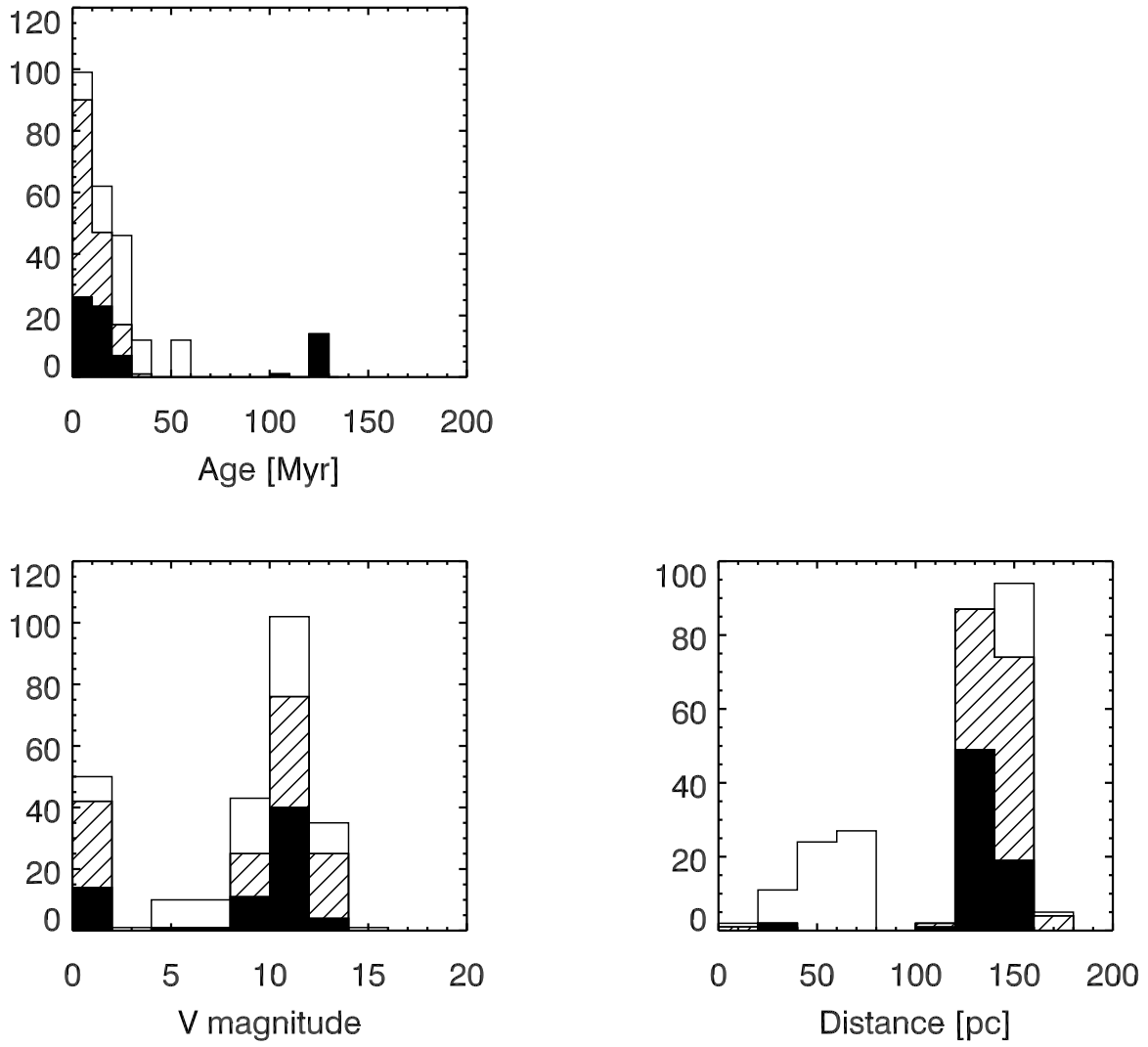


FIG. 2.— Histograms of the properties of the SIM-YSO sample. The slashed and black bars show those targets potentially eliminated and remaining, respectively, after cuts from photometry or nearby companions. The white bars represent those targets yet to be observed in the precursor surveys.

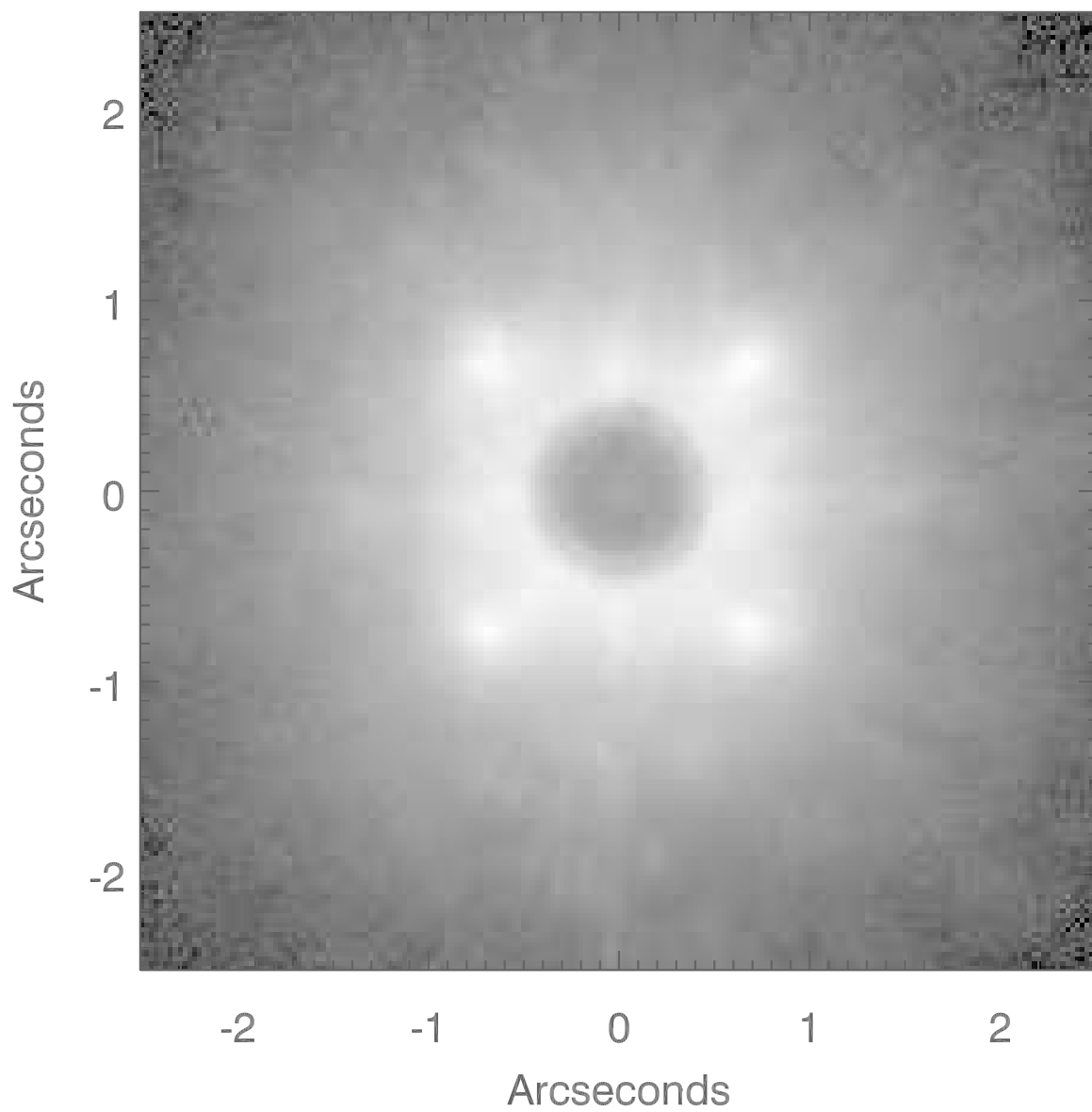


FIG. 3.— Stretched greyscale image of LkCA19 highlighting the poisson spot and waffle pattern inherent in the Palomar AO+coronagraph PSF. North is up and East is to the left.

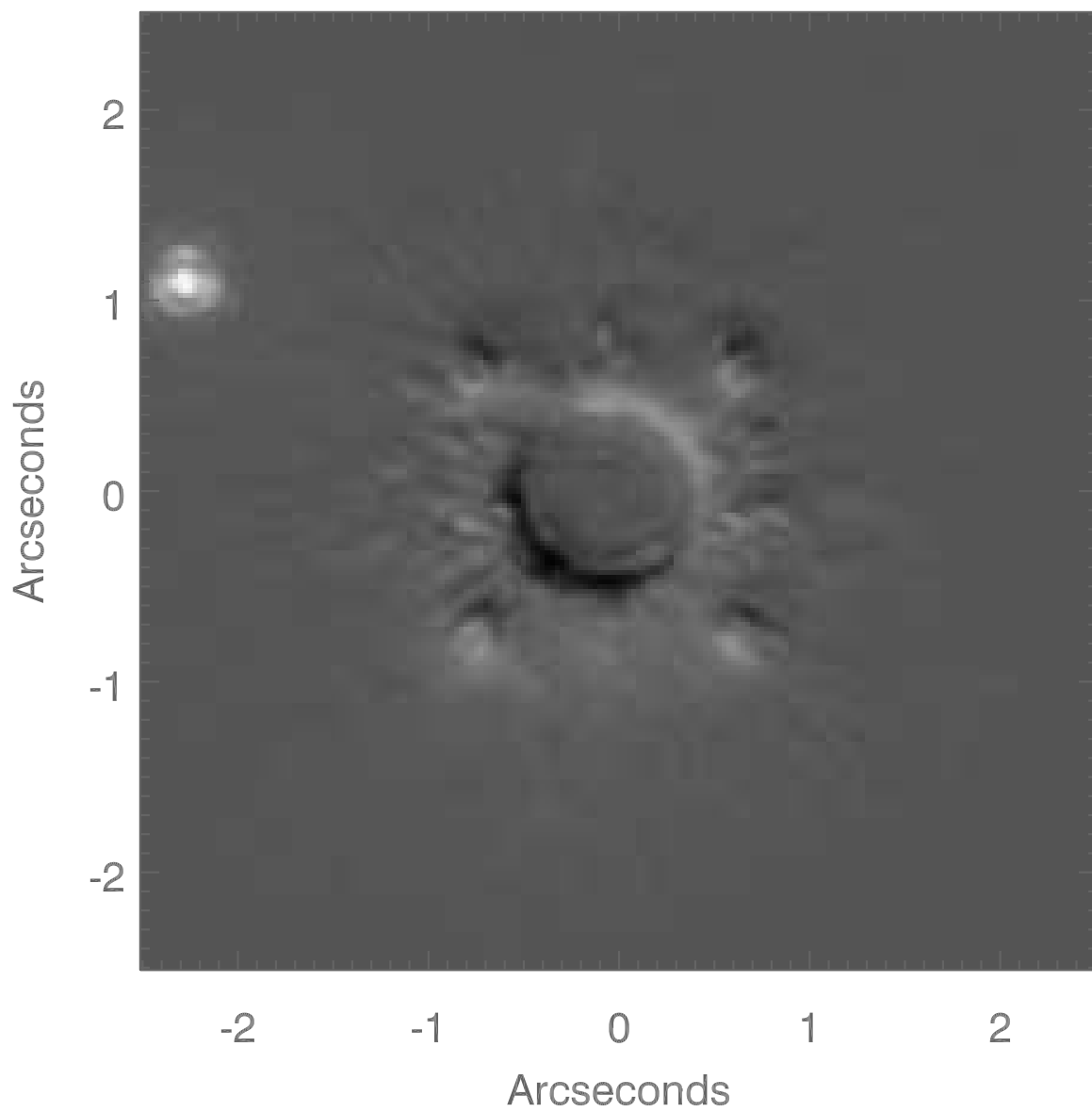


FIG. 4.— Greyscale difference image of GK Tau and V830 Tau. The apparent companion to GK Tau is  $2.4''$  away but is most likely a background star due to its blue colors and non-common proper motion. North is up and East is to the left.

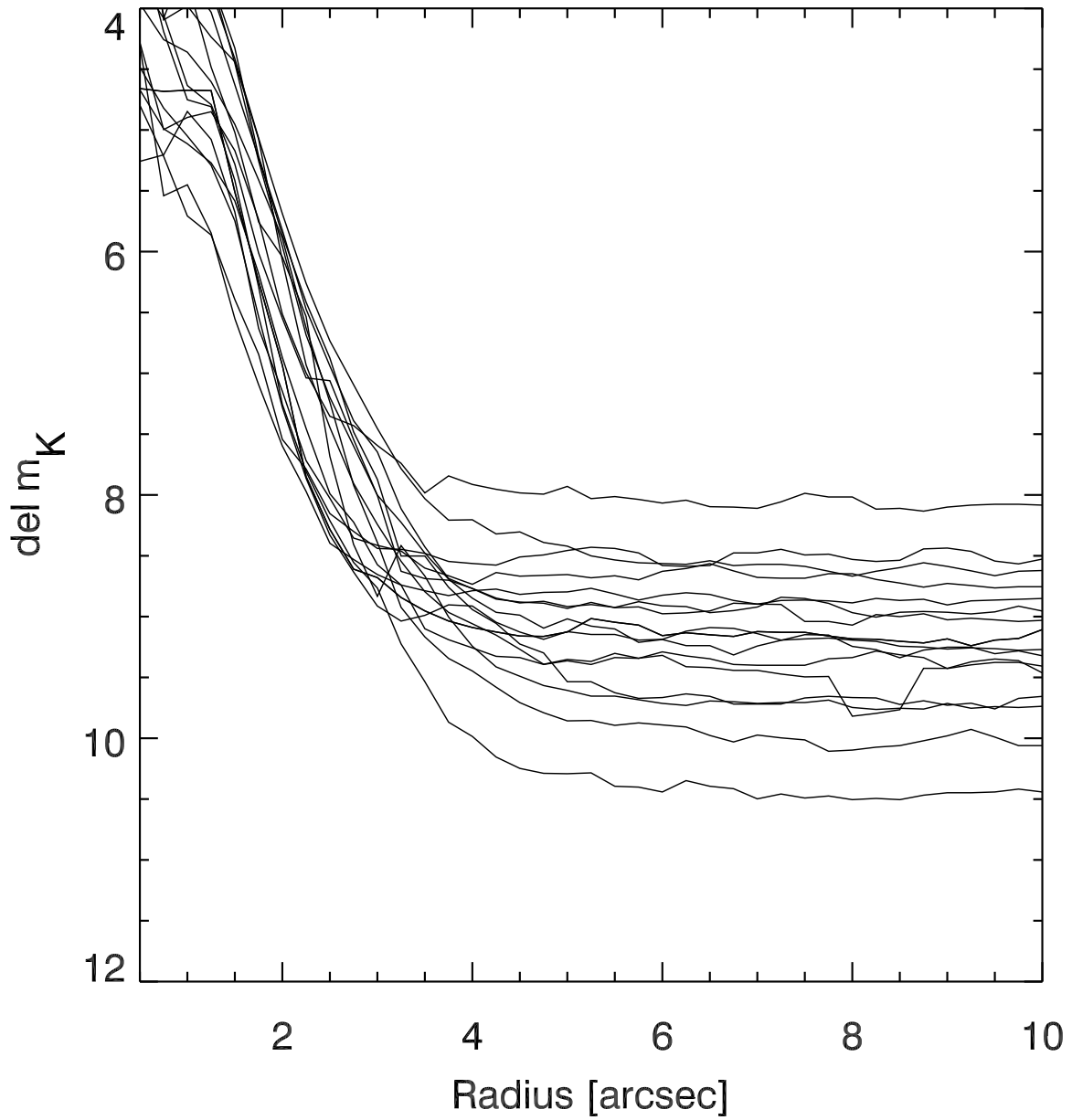


FIG. 5.— Plot of the contrast in  $\Delta K_s$  magnitude detectable in the PHARO images as a function of separation from the target.

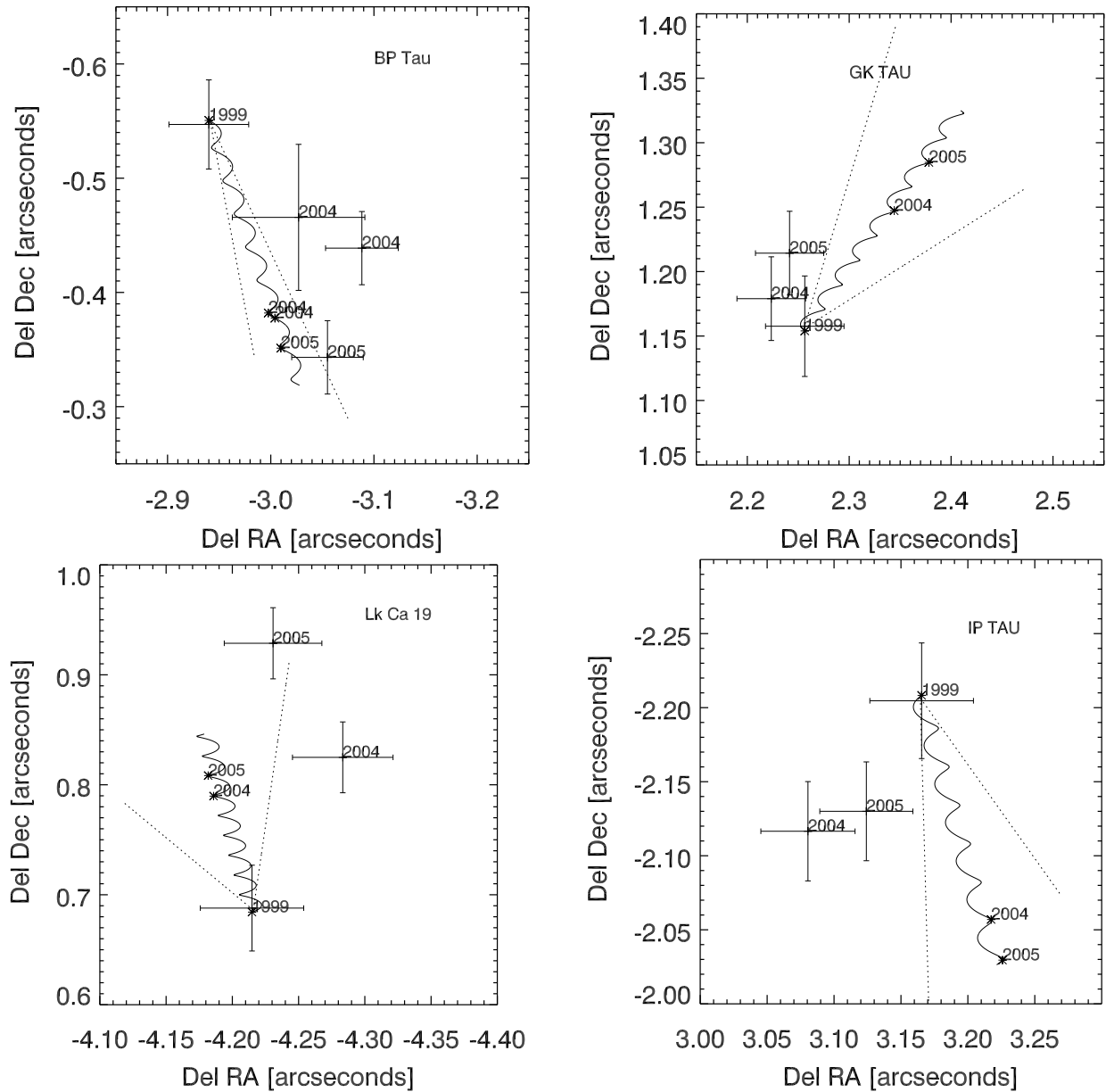


FIG. 6.— Plot of the offset in RA and Dec between BP Tau, GK Tau, IP Tau, and LkCa19 and their companion candidates. The WFPC 2 data point taken in Jan 1999 is used as the initial data point. Each measured offset is noted with a cross and an epoch label. The curvy solid line shows the expected motion of the star assuming measured proper motions from Frink et al. (1997). The expected offset of the companion if it were a steady background object is labeled on the proper motion curve with epoch values (2004,2005). Table 5 lists the reduced  $\chi^2$  values associated with fits to the data points which assume the companion candidates has common and non-common proper motion with their primary stars.

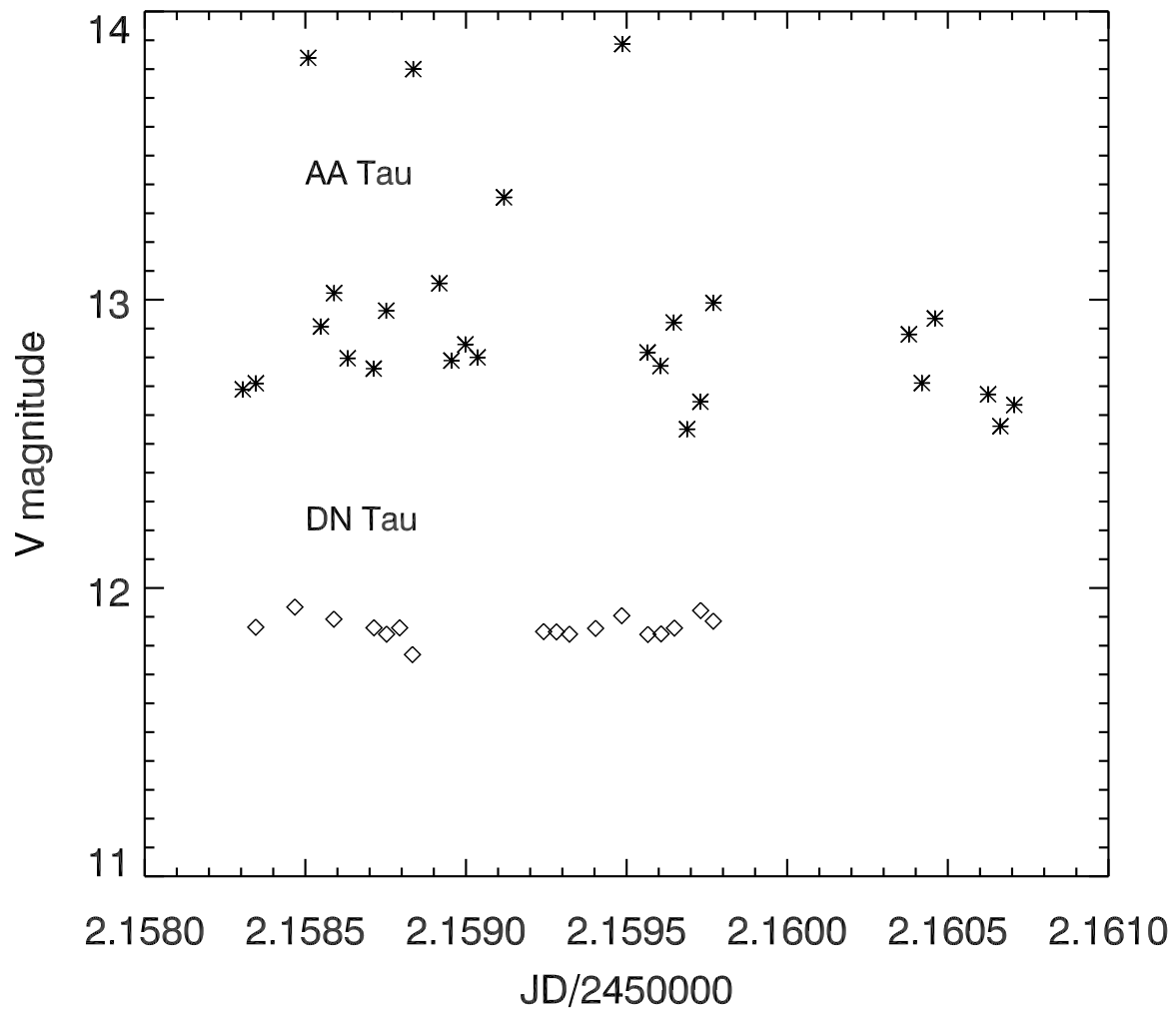


FIG. 7.— Plot of the V band photometry taken for AA Tau and DN Tau. The standard deviations of the photometry for these two sources is 1.5 and 0.17 mag, respectively, making the first source a problematic SIM-YSO target

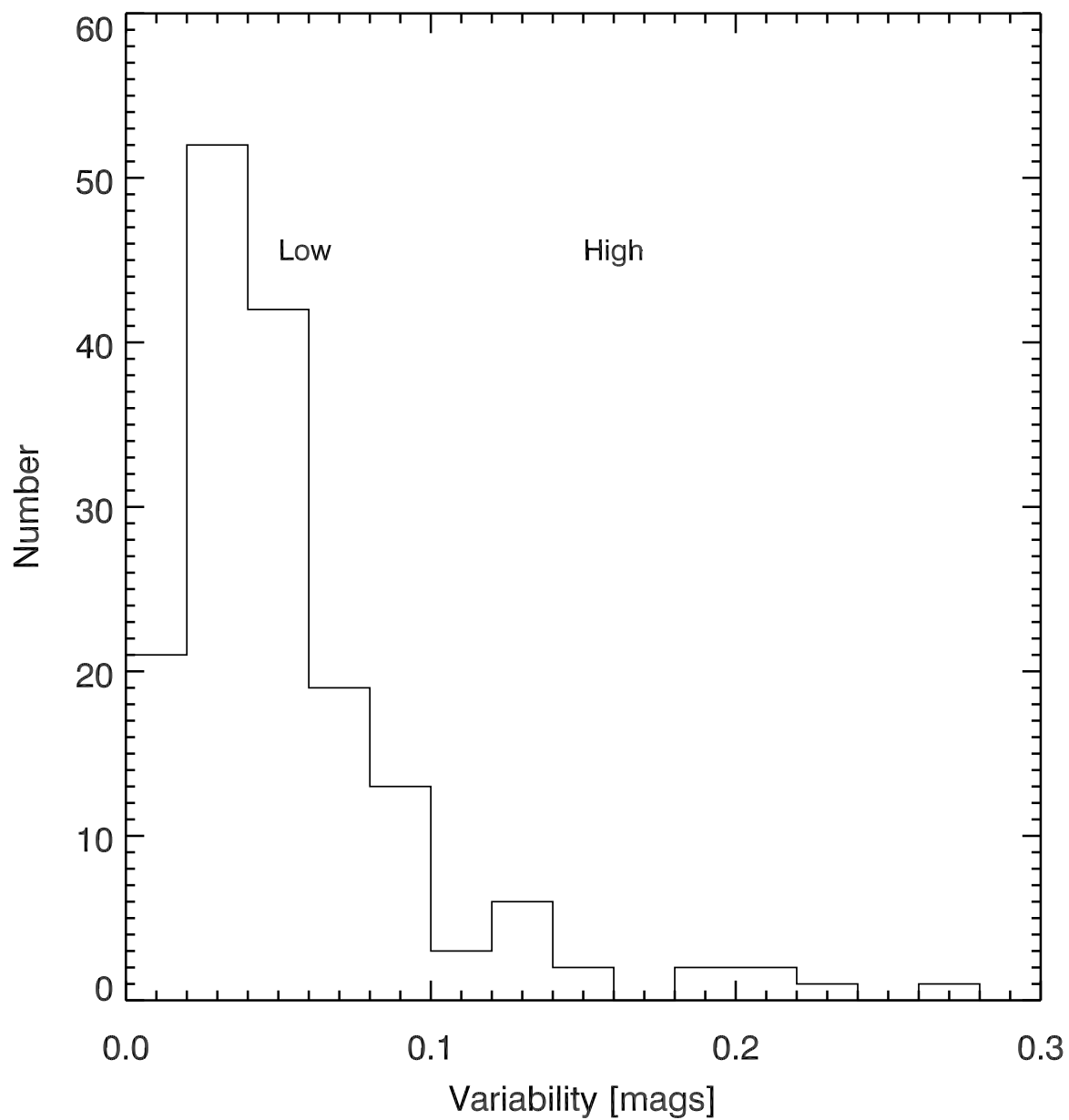


FIG. 8.— Histograms of the standard deviations of the flux variations observed in both the Northern and Southern photometry surveys. A deviation of  $> 0.05$  magnitudes is considered too high for the SIM-YSO targets.

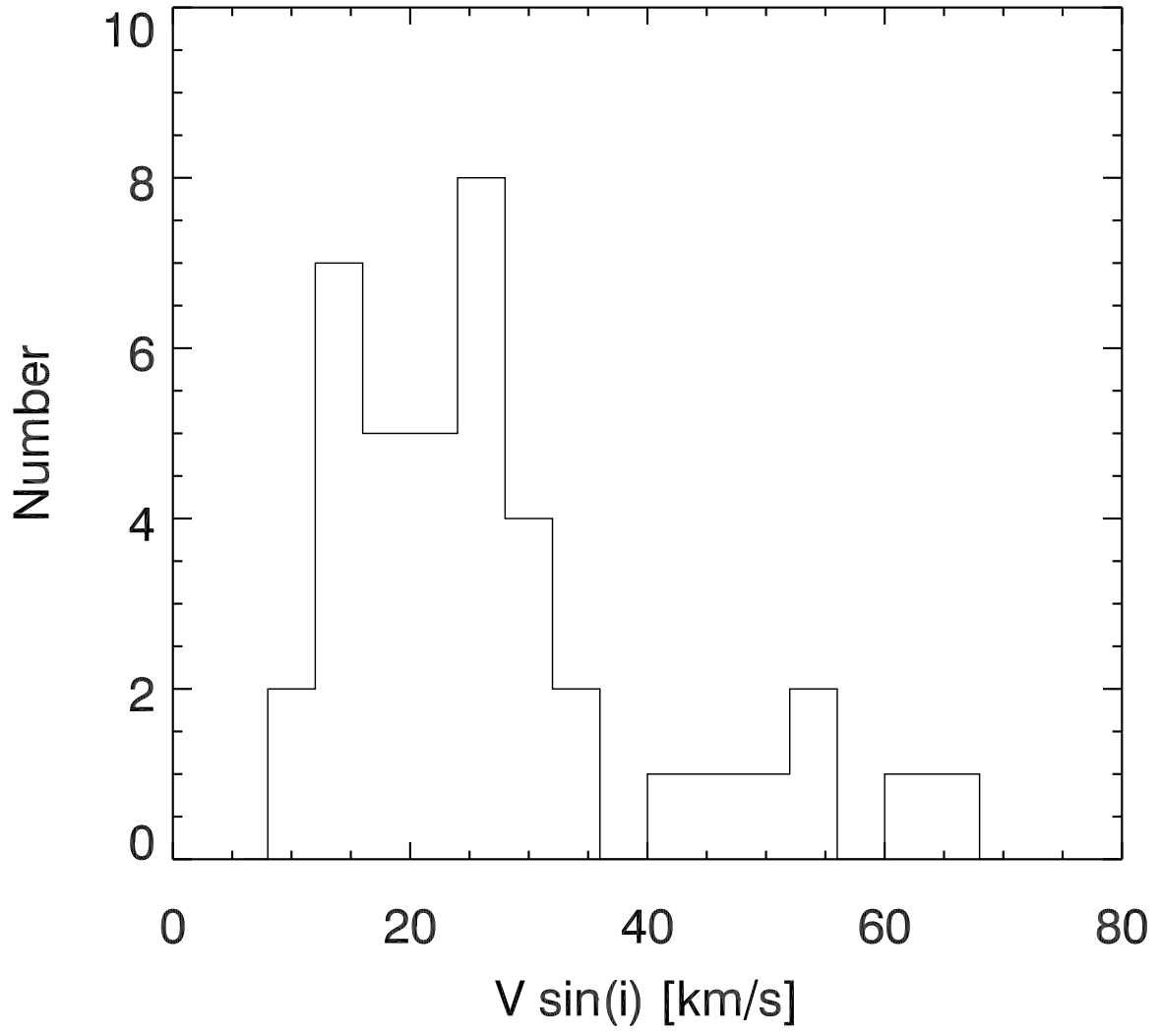


FIG. 9.— Histograms of the values of  $v \sin(i)$  estimated from the Sco Cen sample.